INTERNATIONAL ATOMIC ENERGY AGENCY
UNITED NATIONS EDUCATIONAL, SCIENTIFIC AND CULTURAL ORGANIZATION
INTERNATIONAL CENTRE FOR THEORETICAL PHYSICS
I.C.T.P., P.O. BOX 586, 34100 TRIESTE, ITALY, CABLE: CENTRATOM TRIESTE
UNITED NATIONS INDUSTRIAL DEVELOPMENT ORGANIZATION
INTERNATIONAL CENTRE FOR SCIENCE AND HIGH TECHNOLOGY

SMR: 630/9

MINIWORKSHOP ON NONLINEARITY:
Dynamics of Surfaces in Nonlinear Physics

(13 - 24 July 1992)

"Fractals and Multifractals in Fluid Turbulence"

presented by:

K.R. Sreenivasan
Mason Laboratory
Yale University
P.O. Box 2159
New Havan, Connecticut 06520
U.S.A.

Annu. Rev. Fluid Mech. 1991. 23:539-600

FRACTALS AND MULTIFRACTALS IN FLUID TURBULENCE

K. R. Sreenivasan

Mason Laboratory, Yale University, P.O. Box 2159, New Haven, Connecticut 06520

KEY WORDS: scale similarity, interfaces, cascades, turbulent shear flows, wavelet analysis, statistical mechanics

> The theory of . . . lines and surfaces, for example, has long been recognized as an important branch of geometry, but in treatises on motion it was regarded as lying as much outside of the subject as the four rules of arithmetic or the binomial theorem. . . . geometry itself is part of the science of motion, and [that] it treats, not of the relations between figures already existing in space, but of the process by which these figures are generated by the motion. . . . This method of regarding geometrical figures seems to imply that the idea of motion underlies the idea of form. . . .
>
> James Clerk Maxwell (1879), in his review of Thomson and Tait's *Treatise on Natural Philosophy*

1. INTRODUCTION

1.1 *Scope*

This review is about lines, surfaces, and volumes in turbulent flows and the various measures distributed on them. We limit the discussion to the questions of how fractals and multifractals can be used in this context, and of how much dynamical information we may obtain from this exercise. The subject is a relatively recent addition to studies in turbulence.

The following examples are typical of one class of physical situations with which we are concerned: An initially straight line of hydrogen bubbles placed in a high-Reynolds-number turbulent flow evolves into a complex shape that appears kinked in all three dimensions and on many scales. The surface separating two species (reacting or nonreacting) in a turbulent

0066-4189/91/0115-0539$02.00

flow, even if initially smooth, evolves into a complex pattern. Turbulent jets, flames, and cumulus clouds possess similarly complex boundaries. In mathematical terms, these shapes, patterns, and boundaries are examples of *sets*, and our first objective is to develop intuition about their geometric properties in ways that are independent of the Reynolds number (as long as it is sufficiently high); the second objective is to understand the dynamics of the processes leading to the observed geometry.

Another family of issues, much richer in complexion, concerns *singular measures* distributed on sets — by which we roughly mean highly spiked, positive-definite quantities distributed on lines, surfaces, or volumes. One familiar example is the spatial distribution of energy dissipation. It is well known (e.g. Batchelor & Townsend 1949) that this distribution is spatially intermittent, and that the intermittency increases with increasing Reynolds number. Some other examples are the distributions of scalar dissipation, enstrophy (squared vorticity), absolute values of the Reynolds shear stress, and joint distributions of two or more of these quantities. We should like to quantify such singular measures in terms that are invariant with respect to the Reynolds number, and also to shed light on dynamical scenarios leading to such measures.

The tools we employ are fractals and multifractals. Since there is at present no convincing proof that they are the inevitable tools for our purposes, the viability of the approach rests on *experimental evidence*, which is the aspect on which we focus most. The works of Mandelbrot (1972 and later), Chorin (1982 and later), Frisch & Parisi (1985), Benzi et al (1984), Schertzer & Lovejoy (1985, and references therein) must be considered important precursors to the experimental work described here. This review could in principle have been broadened in scope by including applications of fractals and multifractals beyond turbulence. However, even when restricted to fluid-mechanical problems, the material is enormous and cannot be covered in modest space. For an entry to this literature, see, for example, Jensen et al (1985), Tabeling (1985), Van Damme et al (1986), Olinger & Sreenivasan (1988), Turcotte (1988), Mandelbrot & Scholz (1989), and references therein. Needless to say, we do not dwell at all on applications outside of fluid mechanics; for these, the reader may consult Mandelbrot (1982) (who gives a vivacious account), Stanley & Ostrowsky (1985), Halsey et al (1986), Feder (1988), Barnsley (1988), Avnir (1989), Pietronero (1989), Vicsek (1989), and many others.

1.2 *Seeking Scale Similarity in Real Space*

In contrast to the general practice in dynamical systems, where the emphasis is on phase space, we concentrate on the description of turbulence as a frozen object in three-dimensional physical space. This has the operational

advantage that the embedding space is low dimensional — often only planar and line intersections are studied — and so accurate characterizations are generally possible. But this procedure also imposes a fundamental limitation in that the characterizations are of static objects; dynamic processes responsible for the generation of these patterns cannot be understood without the benefit of ingenuity and inspiration.

A common property of the objects mentioned above, whether of the jet boundary or of the energy dissipation distributed in real space, is the coexistence of a hierarchy of scales. As with similar situations in other areas of physics, one first looks for scale similarity — a notion that, broadly speaking, implies that features at one scale are related to those at another by means of one (or several) scaling factors or functions; the basic reason for expecting this in high-Reynolds-number turbulence is that the Navier-Stokes equations possess some kind of scale invariance. (We use scale similarity to embrace self-similarity as well as self-affinity, both of which are discussed more explicitly in the next section.) Much attention in turbulence has been paid to the framework embodied in Kolmogorov's (1941, 1962) hypotheses — see, for example, Monin & Yaglom (1971) — but, despite the approximate verification of these hypotheses by much experimental work, it is becoming increasingly certain that all their facets do not provide the best abstraction of the right physics. This loaded statement will later be taken up partly, but its detailed discussion is a matter deserving of a separate review. Kolmogorov's theory (at least as practiced most often) is analytical in nature, involving wavenumber interactions, whereas the scale similarity explored here is suggested by considerations of eddies in real space: Turbulent eddies are spatially compact structures, not Fourier modes with infinitely extended support.

The idea of similarity in physical space is old — Richardson (1922), for example, expressed it explicitly — but the force of Kolmogorov's theory seems to have oriented attention in later years to wavenumber space. (For a notable exception, see Townsend 1956.) The balance seems to have been reverting to real space in the last two decades or so, but, as noted by Mandelbrot (1982), turbulent structures are still largely described in terms of Euclidean objects such as blobs, rods, slabs, and ribbons — and occasionally in terms of more imaginative, but unhelpful, metaphors such as melons, beans, spaghetti, lettuce, and the like; on the other hand, reality (e.g. Kuo & Corrsin 1972, Kerr 1985, Frisch & Orszag 1990, Everson et al 1990) calls for "in-between" patterns. Mandelbrot (1982) pointed out that scale similarity cannot be built up in traditional descriptions without introducing dubious assertions, whereas scale similarity is the natural attribute of fractals.

We consider in Section 3 the fractal geometry of scalar and vorticity

interfaces in turbulent flows; before doing so, fractals and fractal dimensions are briefly reviewed in Section 2. In Section 4, we discuss the fractal structure of flame surfaces. Multifractal measures are introduced in Section 5, and the measurement and interpretation of multifractal spectra are described in Section 6. In Section 7, we briefly examine the detailed nature of scale similarity in turbulence. The review concludes (Section 8) with a summary.

2. SELF-SIMILAR AND SELF-AFFINE FRACTALS

2.1 *Self-Similarity, Power Laws, and the Fractal Dimension*

The modern physical notion of fractals is largely due to Mandelbrot (1982 and earlier), but the mathematical notion of sets having noninteger dimensions is much older (Hausdorff 1919, Besicovitch 1929). It is interesting that Mandelbrot (1989a) notes that "It [fractal geometry] fails to have a clean definition and unified tools. . . ." To some extent, this vagueness (see Mandelbrot 1982, pp. 361–62) is characteristic of a subject that is still in flux. To continue the quotation: ". . . mathematical language [of fractals] keeps continuing to evolve and to expand with each new use." A gentleman's definition (that is, one with which gentlemen do not argue) is that a fractal object is one whose parts relate to the whole in *some way*. Serious exploration of the meaning of those two italicized words is tantamount to expanding the subject of fractals itself. Our purpose here is best served by heuristic explanations rather than formal definitions.

In the simplest case of a self-similar deterministic fractal, the same prescribed operation is performed repeatedly on a starting object that may be rather simple. For specificity, consider the triadic Koch curve (Figure 1). The starting object—called the initiator—is here a line of unit length. The construction of the Koch curve proceeds by replacing the line by a new shape itself made of line segments; the new shape is called the generator. The construction of the succeeding steps consists of replacing each line segment of the previous step by a scaled version of the generator. In this example, the individual line elements at each step decrease in length by a factor of 3—hence the name triadic. The result of the first few iterations is given in Figure 1. The curve at the end of many iterations would have a wide range of scales. At any stage of construction, the curve possesses the important property that, when a part of it is expanded by a factor 3^n (where n is an integer), it looks the same (except for trivial reorientation) as that obtained n stages previously. Thus comes the notion that self-similar fractals are invariant to dilation.

In nonlinear physics, one often (or almost always) does not have access to details of the construction of a fractal, only to the final form at the end

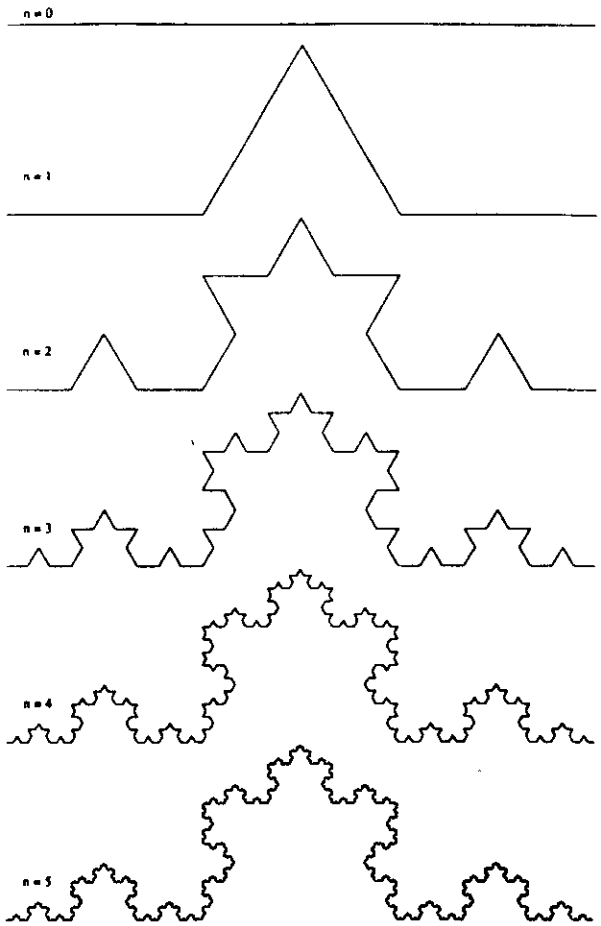

Figure 1 The construction of a triadic Koch curve. The figure is taken from Feder (1988). For a description of other Koch curves, see Mandelbrot (1982).

of an (unknown but large) number of iterations. Consider the Koch curve at the end of many iterations. By estimating the length Λ of this curve at finer and finer resolutions r, one essentially replicates features at various generation levels. The length estimated by a yardstick of unity gives a length estimate of unity, which is the length at the zeroth iteration; a

yardstick or resolution of $(1/3)^n$ yields the length of $(4/3)^n$, which is exactly the length at the nth generation. As the resolution improves, the length keeps increasing. This situation is quite different for a classical line. Its length, as measured by covering it with finer and finer yardsticks, remains the same for all yardsticks smaller than a certain value. In this sense, the fractal curve "has more in it" than an ordinary curve. The intrinsic parameter that quantifies this property is its dimension: The dimension of a fractal curve is more than unity, a fact for which its convolutedness at all scales is responsible. The curve may be so highly convoluted that it effectively covers an area, in which case the curve is said to be space filling with dimension 2. A fractal surface will in general have a dimension greater than 2, but it could have a dimension as high as 3 if it is so highly convoluted as to effectively fill a volume. In this sense, the fractal dimension is a measure of the space-filling ability of a fractal set. The co-dimension, which is the difference between the dimension of the embedding space and the fractal dimension, is a measure of the sparseness of the fractal.

We have seen for the Koch curve that $\Lambda(r/3) = (4/3)\Lambda(r)$, whose solution is of the form

$$\Lambda(r) = r^{1-D}, \tag{2.1}$$

where $D = \log 4/\log 3 = 1.2618\ldots$. The number of length elements required to cover the total length is given by Λ/r and equal to

$$N(r) = r^{-D}. \tag{2.2}$$

It follows that

$$D = \lim N/\log(1/r). \tag{2.3}$$

One can easily convince oneself that the application of (2.3) to lengths, areas, or volumes of Euclidean objects yields the familiar dimensions. D is therefore thought to play the same role for fractal objects and is called the fractal dimension; it can be determined in principle using (2.3), but in general expressions (2.1) (2.3) contain prefactors. In practice, it is thus better to obtain D from the slope in log-log plots of (2.1) or (2.2). Unless one refines the yardstick naturally (by the factor 1/3 in the case of the triadic Koch curve) and partitions the length in a natural way by starting measurement exactly at the beginning of a piece, one finds oscillations in the log-log plot around a mean slope. The prevalence of power laws with respect to the scale of observation in a certain range is commonly used to discern a fractal, especially when the scale similarity is statistical and cannot always be identified by sequential enlargement of segments of the fractal object.

A generalization for the areas and volumes of fractal surfaces and volumes is

$$S \sim r^{2-D}, \qquad V \sim r^{3-D}, \tag{2.4}$$

where D is given by the formula (2.3), with N being the number of area or volume elements of linear dimension r. Note that while the fractal dimension is the most basic property of a fractal, many fractals can be constructed with the same dimension.

2.2 *The Method of Intersections and the Additive Law*

In turbulence research, one is nearly always forced by limitations of measurement technology to work with one- or two-dimensional sections of three-dimensional objects. This leads us to ask, How are the fractal dimensions from such sections related to that of the original object? The general problem of relating the dimension of a fractal object F to those of its intersections has been discussed in the literature, and some results are available for special cases (Marstrand 1954, Hawkes 1974, Mattila 1975, Mandelbrot 1982, Falconer 1984). Roughly speaking, if F is embedded in three-dimensional space and intersected by a thin plane — in practice, about as thin as the finest scale present — the dimension of the intersected set is one less than that of F *provided that the result is independent of the orientation of the intersecting plane*. Similarly, the dimension of line intersections is two less than that of F, again under the provisions that the line be no wider than the finest scale and the result be independent of the orientation of the intersecting line. In the absence of such careful demonstrations, the additive law cannot in general be used (see, for example, Bunde et al 1987). Adequate demonstrations have been possible for some aspects of turbulence and are discussed at appropriate places.

Finally, it should be said that these intersections will be empty very often if F is extremely sparse. A large number of intersections will then be necessary to establish the properties of F.

2.3 *Some Methods for Fractal-Dimension Measurement*

Mandelbrot (1982) discusses several methods for determining the dimension of the fractal boundary. Another useful discussion can be found in Section 2 of Avnir (1989). In a planar digital image containing a fractal boundary, the co-dimension method involves computing the smallest distance from each pixel to the boundary and determining the number of pixels $N_c(r)$ lying within a distance r from the boundary. The slope of this straight region in log-log plots of $N_c(r)$ versus r is the co-dimension D_c of the boundary; its fractal dimension is $2 - D_c$. In the box-counting method, one covers the whole plane with square elements of varying sizes and counts the number $N(r)$ of elements containing the boundary. The negative slope of log $N(r)$ vs log r yields the dimension of the fractal boundary. In

general, box-counting methods are far more efficient than co-dimension methods. Other methods involve following the boundary with dividers of varying lengths and obtaining the corresponding apparent lengths; slopes in log-log plots [see (2.1)] yield the fractal dimension. This method is usually difficult for multivalued and fragmented boundaries, but one can use suitable coarse-graining filters at various scales.

All these techniques examine a single object with various resolutions, but other methods can be used when one has access to various-sized objects belonging to the same class (e.g. cumulus clouds of different sizes). The so-called perimeter-area method is one such technique. For an object with a fractal boundary, the perimeter continues to increase with the resolution of measurement, whereas the area asymptotes to a finite value. Mandelbrot (1982, p. 110) shows that, *for some fixed resolution small enough to measure the smallest sized object accurately*, the perimeter P and the area A of such objects of various sizes follow the relation

$$P \sim A^{D/2}, \tag{2.5}$$

where D is the boundary dimension. Consistent with experience, $D = 1$ for Euclidean objects.

For a boundary evolving dynamically, one can obtain the area swept by the boundary at two closely spaced times and use the co-dimension method. Not all of these definitions need give the same result.

2.4 *Self-Affine Fractals*

Consider for example a turbulent velocity component measured as a function of time at a single point. As shown in Figure 2, it looks rough, like the boundary of a random fractal (e.g. a coastline), but with the difference that the two axes correspond to different physical quantities – velocity and time – that are intrinsically different. One can choose different units for the two axes to make the trace look either very steep or nearly smooth. Similarly, from a scalar field in two dimensions, one can construct a mountainlike structure in which the height at each point equals the magnitude of the local concentration. Again, the height (on the one hand) and the two spatial coordinates (on the other) are intrinsically different and independent, so that the mountain can be made to look jagged or relatively smooth depending on the choice of units for the two quantities. In general, whenever different quantities involved in such constructions scale differently, the notion of self-similarity contained in Equations (2.1)–(2.3) will not be adequate; to describe these phenomena, one needs the more versatile machinery of self-affinity. An affine transformation is one that transforms a variable $\xi = (x_1, x_2, x_3, \ldots)$ into a new one $\zeta = (ax_1, bx_2, cx_3, \ldots)$, where the scaling ratios $a, b, c, \ldots$ are all different. If a subset of a process is

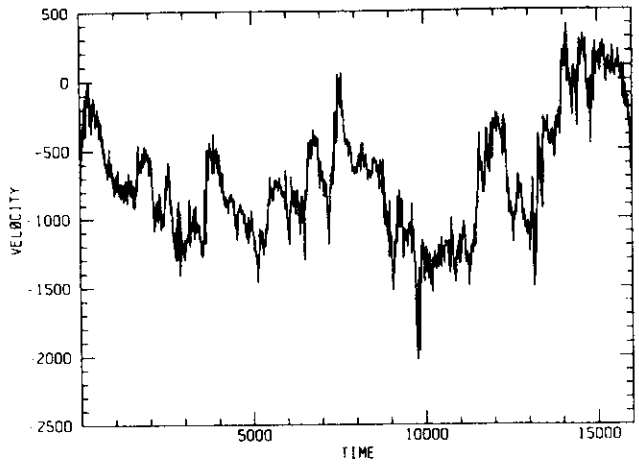

Figure 2 A turbulent velocity signal measured using standard hot-wire anemometry 18 m above the ground in an atmospheric surface layer. Time and velocity are plotted in arbitrary units.

similar to the whole under an affine transformation, the process is said to be self-affine. Mandelbrot (1985, 1986) has discussed self-affine fractals and introduced recursively self-affine fractals (see also Voss 1989).

One cannot define similarity dimension for even the simplest self-affine fractal curves. If one evaluates this dimension mechanically, pretending the curve in Figure 2 to be like a coastline, the value depends on the expansion used for one quantity relative to the other. If, for example, the time scale is stretched enough to render the signal to appear as a collection of smooth increments, it is intuitively clear that the dimension (called the global dimension) will be unity. If, on the other hand, the ordinate is stretched over a range of values, one can define the usual fractal dimension according to (2.1). This is the so-called local dimension of the self-affine fractal. As pointed out by Mandelbrot (1986), more than one dimension is necessary to characterize self-affine fractals. For the most part in this review, we do not concern ourselves with self-affine fractals – partly because not much work has been done beyond that mentioned, say, by Turcotte (1988) and Voss (1989) and partly because many subaspects of self-affine fractals possess self-similarity. For example, while the velocity trace of Figure 2 is self-affine, there are reasons to believe (Section 3.2) that some of its level sets (that is, the sets of points obtained by various level crossings) are self-similar. There is much scope for further work here.

3. FRACTAL DIMENSION OF SURFACES IN TURBULENT FLOWS

Sreenivasan & Meneveau (1986) have shown, using their own data as well as those of Corrsin & Karweit (1969), that the evolution of material lines in grid turbulence can be interpreted in terms of the fractallike properties of turbulence. There are few data on this topic beyond those contained in these two sources. On the other hand, there has been much work on surfaces in turbulent flows since 1986, and so we concentrate on that aspect.

3.1 *The Scalar Interface*

A passive scalar introduced into a turbulent flow gets dispersed by turbulence, but the scalar-marked region possesses, at high Reynolds numbers, a sharp boundary. This is the scalar interface. We are interested in the properties of this interface, partly as an object of interest in its own right and partly because of its relevance to mixing and combustion.

The existence of the scalar interface has been known for a long time (Corrsin & Kistler 1955). Its complexity was particularly well demonstrated by Dimotakis et al (1983), who obtained well-resolved photographs of jet sections with the use of the laser-induced fluorescence (LIF) technique. More recently, Prasad & Sreenivasan (1989, 1990a) obtained quantitative two- and three-dimensional LIF images of the scalar field in wakes and jets, concluding that the interface, in spite of its fragmented appearance in two-dimensional sections, is largely contiguous. They also noted that even though the large-scale structure of the interface is apparent from one parallel plane to the next, small-scale variations are so prevalent that any two neighboring sections of the interface have very little correlation on the average.

In liquid flows in which various dyes have been used as scalars, the Schmidt number ($Sc = \nu/k$, where ν is the kinematic viscosity and k is the mass diffusivity) is of the order 1000. This leads to two distinct scaling regions. Speaking loosely for the present, one of them (to be called the K-range below) occurs between the integral scale L and the Kolmogorov scale η, and the other (to be called the B-range) occurs between η and the Batchelor scale $\eta_b = \eta Sc^{-1/2}$ (Batchelor 1959). The physics as well as the techniques of dimension measurement are quite different for the two cases, which are therefore best discussed separately.

3.2 *The Dimension in the* K*-Range*

The definition of the interface usually entails some edge-enhancement techniques. There is a vast literature on the subject in the domain of

artificial intelligence and pattern recognition (e.g. Canny 1986, and references therein). In our specific context, Prasad & Sreenivasan (1989) and Saylor (1989) have investigated several edge-enhancement methods, and they essentially concluded that as long as the images are relatively noise free, the simple procedures of setting a proper threshold on the pixel intensity marks the boundary at least as well as the more sophisticated techniques.

Prasad & Sreenivasan (1990a) mapped the interface in a volume of order $700\eta \times 600\eta \times 32\eta$, with resolution of order 4η, and used this three-dimensional data base for dimension measurements in the K-range. Box counting in three dimensions produced a straight region in the log-log plot; the dimension was found to be 2.35 ± 0.05 for both jets and wakes.

Two-dimensional digital images from LIF intersections provide a good data base for such measurements because of the good signal/noise ratio and their relatively extensive size. (The images should not be too extensive, however, because of streamwise inhomogeneity and consequent variation of scales in the downstream direction.) Prasad & Sreenivasan (1990b) have discussed the various steps necessary to obtain low-noise images. It is crucial to do this first step well to avoid ambiguous conclusions later. Such sections have been obtained in the jet (Sreenivasan & Meneveau 1986, Prasad & Sreenivasan 1990b) and mixing layers (Ramshankar 1988, 1989). Dimotakis et al (1983) have obtained comparable LIF photographs of jet sections, and Sreenivasan & Aronstein (1985) and Sreenivasan & Meneveau (1986) have obtained smoke photographs of boundary-layer sections. Figure 3 gives an example of a jet image. The computer-drawn boundary of the image, obtained by setting the threshold at a pixel brightness level deemed satisfactory by visual inspection, is shown in Figure 4. The log-log plot of $N(r)$ versus r is shown in Figure 5*a*. The slope gives a fractal dimension of 1.36 for the boundary. By the additive law, the interface dimension is 2.36. A dimension histogram constructed from 70 images has yielded a mean dimension of 2.36 and a standard deviation of 0.03.

The classical inertial scaling in *frequency spectra* is restricted to scales $\eta \ll r \ll L$ and is negligible in extent at the Reynolds numbers of the measurements described above. On the other hand, the straight part in Figure 5*a* extends from the smallest scale resolved here (approximately twice the average Kolmogorov scale) to a scale on the order of the nozzle diameter. Even though the scaling for each interface is good, the scaling exponent (i.e. the dimension) fluctuates from one realization to another. Prasad & Sreenivasan (1989) found that the difference between the extreme values of the dimension is too large to be attributed to experimental uncertainties, and thus they concluded that the fluctuations are a real feature of the physics. One possible effect of these fluctuations is to degrade

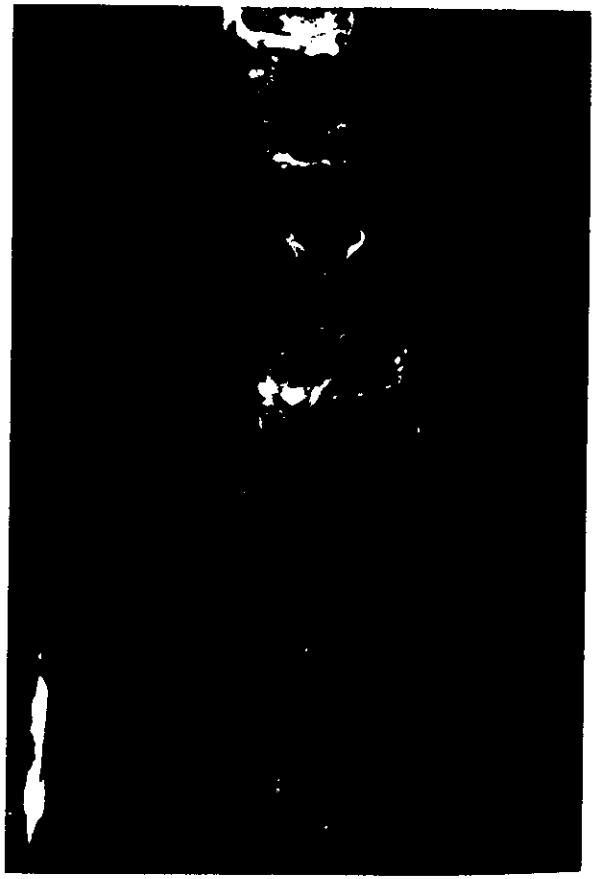

Figure 3 A two-dimensional image of an axisymmetric water jet, obtained by the laser-induced fluorescence (LIF) technique. A Nd:YAG laser beam shaped into a sheet of 200–250 μm thickness using suitable lenses was directed into a water tank into which the jet fluid was emerging from a well-contoured nozzle and standard upstream flow management; the jet fluid contained small amounts of uniformly dispersed fluorescing dye (sodium fluorescein). The fluorescence excited by the laser radiation was captured on a digital camera (a charge-coupled device, with a pixel array size of 1300 × 1035). The pixel intensity in the digital image was linearly related to the concentration of the dye. Different shades of gray in the figure qualitatively reflect different concentration levels. The laser had a power density of about 2×10^7 J s^{-1} per pulse and a pulse duration of 10 ns. The flow is thus frozen to an excellent approximation. The region in the image extends from 8 to 24 nozzle diameters. The nozzle Reynolds number was about 4000. The laser-sheet thickness was between $\langle\eta\rangle$ and $2\langle\eta\rangle$, where $\langle\eta\rangle$ is the Kolmogorov thickness averaged over the image (from Prasad & Sreenivasan 1990b).

Figure 4 The two-dimensional image of Figure 3, with the computer-generated boundary representing the interface between the scalar-marked region and the ambient unmarked fluid in the tank. The boundary was generated by setting a threshold on the pixel intensity in the digital image. The boundary is generally realistic, but (since some minor ambiguities do remain) sensitivity checks are essential; see Figure 5 (from Prasad & Sreenivasan 1990b).

scale-similarity when box counting is performed over many images before obtaining log-log plots. The basic physical question, then, is to determine the source of these fluctuations. We encounter similar fluctuations elsewhere in this review, and so its discussion is best relegated to a later section (Section 6.5).

Figure 5*b* shows the boundary dimension as a function of the threshold on the intensity. It appears that the fractal dimension of the boundary is essentially threshold independent over a wide range. Interfaces determined from photographs show greater sensitivity to thresholds, as shown in

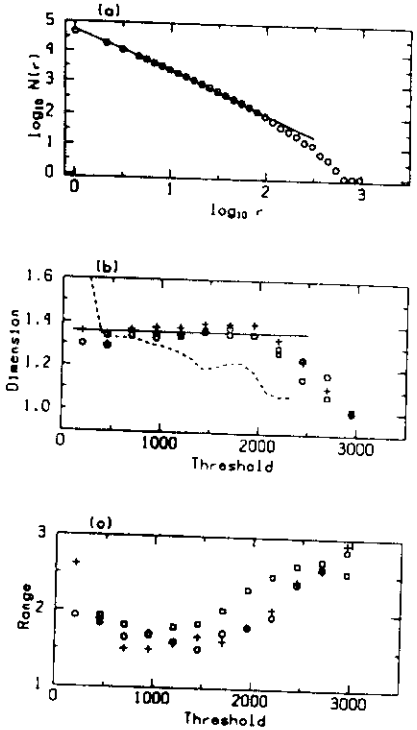

Figure 5 (*a*) A typical log-log plot of the number $N(r)$ of the square area elements ("boxes") of size r containing the boundary versus the box size r. The negative slope of the straight part gives the boundary dimension (= 1.36). (*b*) The dimension as a function of the threshold chosen to generate the interface. The abscissae ranging from 0 to 4096 are the nominal dynamic range of the digital camera. Over some fraction of the concentration levels chosen for the boundary generation, the dimension does not vary much. Also shown in the graph is the threshold variation in an image obtained by digitizing a jet photograph (*dashed line*), with the abscissae rescaled to match the range of the digital camera. Because the gray levels in ordinary photographic film are poorer in dynamic range than the best digital cameras, there is a greater uncertainty in defining the boundary by the threshold method, leading to a greater sensitivity to threshold—typically as shown. Figure (*c*) shows that the scaling range [= $\log_{10}$(outer cutoff/inner cutoff)] has definite sensitivity to the threshold (for a relevant point, see Figure 6). The available scaling L/η in the K-range is about 250 for the Reynolds number of the jet. Different symbols in (*b*) and (*c*) correspond to different realizations of the jet at the same Reynolds number (from Prasad & Sreenivasan 1990b).

Figure 5*b*. It must, however, be remarked that this variation is different for different photographs, depending on the processing details.

Figure 5*c* shows that the scaling regime is smaller for intermediate thresholds. In fact, for these thresholds, there is an uncertainty about the existence of good scaling because the log-log plots are somewhat rounded. The worst case is the isoconcentration contour corresponding to the mean level over the entire picture, shown in Figure 6*a*. The scaling for this boundary is shown in Figure 6*b*. It may be inferred from Figure 6 that boundaries close to mean concentration level, encompassing well-mixed regions, are not good candidates for fractallike description. Notice that in longitudinal images with good signal/noise ratio, the axial diminution of concentration levels has no effect on the definition of the interface (because it is defined by a concentration level just above the noise), but it could strongly affect the definition of other isoconcentration contours, especially those close to the image mean. At very large distances from the nozzle, the signal is small and the identification of any isoconcentration contour becomes difficult; one experiences the most difficulty in the definition of the contour corresponding to the image mean. The rounding of log-log plots for intermediate levels may in part be an artifact of the jet spread and the dilution of dye concentration in the axial direction, although sections orthogonal to the jet axis show no strong variations in either the extent or the quality of scaling. The tentative thinking is that *if appropriate rescaling is done to account for this inhomogeneity* [for example, in the manner used by Everson et al (1990)—see Section 7], the sensitivity to the threshold might be less evident, and that isoconcentration surfaces not too close to the mean concentration level are fractallike.

For the additive law to hold, intersections in different orientations must have the same fractal dimension. Prasad & Sreenivasan (1990b) obtained interface sections off-axis as well as normal to the jet axis and showed that the dimension of the boundary in each case was essentially the same. This suggests that *strong* anisotropic effects are confined essentially to the largest scales—on the order of the flow width and larger. The residual anisotropy of smaller scales obeying fractallike behavior appears through unequal ranges of scale similarity in two orthogonal planes, but not through the dimension itself. This issue, however, deserves closer scrutiny.

The validity of the additive law for line intersections has been examined by Sreenivasan & Meneveau (1986) and Sreenivasan et al (1989a). In Figure 7, the jet boundary in a planar intersection is marked in the usual way, and its intersection with a line is also shown. A majority of lines through the figure intersect the boundary at different sets of points, whose dimensions can be measured, for example, by box counting. The additive law allows us to interpret this result to be two less than the dimension of

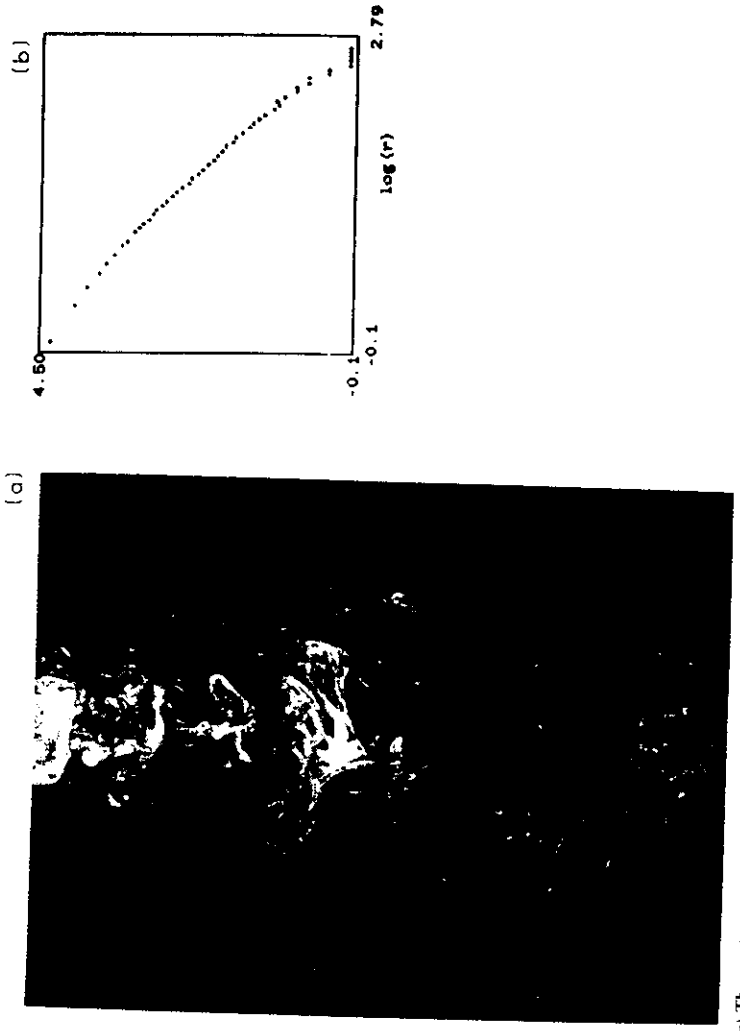

Figure 6 (*a*) The contour corresponding to the average concentration in the image. This contour has a reduced extent of scaling (see Figure 5*c*), as well as a reduced quality of scaling [Figure 6*b*, which plots log $N(r)$ versus log r]. These features may in part be artifacts of the downstream growth of the jet and the consequent dilution of concentration (from Prasad & Sreenivasan 1990b).

Figure 7 The boundary of a jet in a two-dimensional intersection, and its intersection with a line in the plane of the two-dimensional section. The points of intersection form a set whose dimension can be calculated by box counting. Sreenivasan et al (1989a) have calculated the dimension as a function of the vertical and horizontal positions, as well as the orientation, of line cuts, and they found the dimension to be consistently the same.

the interface (surface embedded in three-dimensional space). Sreenivasan et al (1989a) showed that, in some range, the dimension was largely independent of the position of the line or its orientation, and that the result was quite close to two- and three-dimensional ones (see Table 1). However, log-log plots for one-dimensional intersections contain larger scatter, primarily because of the lack of sufficient data: Sections perpendicular to the flow axis are naturally limited by the flow width, and data extents of more than a few tens of integral scales in the streamwise direction are hard to

Table 1 Summary of fractal dimension measurements in classical turbulent flows (from Prasad & Sreenivasan 1990b)

	Scale range between η and L			
	Method of measurement			
Flow	1-D cuts[b]	2-D images	3-D images	Scale range between[a] η and η_b
Round jet	2.36	2.36	2.36	2.7 (Sc = 1930)[c]
Plane wake	2.40	2.36	2.36	2.7 (Sc = 1930)
Plane mixing layer	2.39	2.34		
Boundary layer	2.40	2.38		

[a] All measurements are from one-dimensional cuts, with Taylor's hypothesis (see text)

[b] These one-dimensional measurements for jets and wakes were made mostly by taking cuts of two-dimensional images. Some estimates were also made using Taylor's hypothesis. Note that one-dimensional measurements often yield slightly higher values for the dimension, but experimental uncertainties preclude us from attaching significance to this result. The mean value and statistical error bars, deduced from many measurements, are 2.36 ± 0.05. The slight difference from one flow to another may or may not be significant; the present thinking is that they are not

[c] The Schmidt number is taken from Ware et al (1983). Typical error bars for this estimate are ± 0.03

image while maintaining small-scale resolution. Further, the significant streamwise inhomogeneities in such large images will have to be removed by some rescaling, as discussed in Section 7.

On the other hand, there is a long tradition in turbulence research of regarding a temporal record obtained by a single-point probe as a spatial cut. This is Taylor's frozen-flow hypothesis, according to which turbulence patterns convect with the mean motion without distortion. One can take very long temporal records with ease. While this procedure stabilizes the statistics, it also introduces well-known uncertainties. Much of the literature on Taylor's hypothesis concerns the interpretation of frequency spectra as wavenumber spectra (e.g. Lumley 1965, Monin & Yaglom 1971, Antonia et al 1980, and references therein), and the precise effect on the dimension measurements is not understood. Large fluctuation velocities mean that a random stretching of the time axis must be performed to interpret a temporal trace as a spatial cut, but this has not been attempted. The empirical facts (Sreenivasan & Meneveau 1986; see also Gouldin et al 1988) are as follows: (*a*) Short records (of order $10L$) show fractallike behavior, but this property is lost when viewed on very long scales. The situation is worse for jets than wakes, presumably because a typical ratio of the fluctuation velocity to the translation velocity in jets is about two orders of magnitude larger than that for far wakes. (*b*) For threshold levels comparable to the mean value of the signal, the log-log plots are in general

rounded, especially for isovelocity contours. In fact, there are indications (e.g. Sreenivasan et al 1983) that in long one-dimensional cuts, fluctuations close to the signal mean tend to be noiselike (obeying Gaussian statistics) rather than fractallike. (*c*) The recommended procedure – although unsatisfactory from a fundamental point of view – is to consider many relatively short segments of data and average the slopes. This procedure gives results generally consistent with the two-dimensional ones.

The observation that Taylor's hypothesis approximately preserves geometric scaling on short time scales is both interesting and useful. In particular, it has been shown (Sreenivasan et al 1989a) that the dimension is the same for temperature interfaces in air flows and for dye interfaces in liquid flows in the K-range, even though heat diffuses about three orders of magnitude faster in air than does a typical dye in water. The analysis of the time record is interesting in its own right, independent of its relation to the spatial cuts, but here we do not expand on its nonfractal nature.

Dimension measurements have been made in other classical shear flows. The principal results are summarized in Table 1. Note that within the uncertainty of measurement, serious credence cannot be given to differences in values estimated from one- and two-dimensional sections or to variations from one flow to another. To a good first approximation, the fractal dimension of scalar interfaces in the K-range is 2.36 ± 0.05 for all fully turbulent flows considered here. (The mean value is the same for all these flows, but the error bar is higher when data from all flows are grouped together.)

It is important to establish the Reynolds-number dependence of this result. Prasad & Sreenivasan (1990b) analyzed LIF images of jets up to Reynolds numbers of about 15,000. The interpretation of these results was hampered by the fact that the jet sections were substantially fatter than the Kolmogorov scale (because of constraints of light-sheet thickness). To interpret such data, these authors studied the effect of taking sections of different relative thicknesses at a Reynolds number of 4000 and showed that the dimension decreased much like a Gaussian from the thin-section value. The least-squares fit to the data was of the form $D = D_0 + a\exp(-h^2/2\sigma^2)$, where $D_0 = 1.22$ is the dimension of the interface projected onto a plane, $a = 0.147$, $\sigma = 6.82$, and h is the thickness of the slab nondimensionalized by the Kolmogorov thickness. [From standard results available on fractal sets (see, for example, Falconer 1984) one can merely conclude that the dimension in the projection should lie between 1.36 and 1; the former is the true dimension of the interface boundary, whereas the latter is the dimension of a classical line. Assuming that this relation was also valid for high Reynolds numbers, Prasad & Sreenivasan (1990b) inferred from their thick-section data that the dimension of the interface

was 2.36—independent of the Reynolds number as long as it was "sufficiently high." A rigorous upper bound evaluated for the dimension of scalar isosurfaces is 2.5 (Constantin 1990).

The Reynolds-number dependence at much lower values was examined by Ramshankar (1988, 1989) for a temporally developing mixing layer and by Prasad & Sreenivasan (1990b) for a plane wake. The dimension here makes a transition from the low-Reynolds-number value of 2 for the smooth interface to the asymptotic value of 2.36. A typical intermediate variation, shown in Figure 8 for the mixing layer, is characterized by an abrupt initial rise of the dimension. A similar Reynolds-number-variation of a related scaling exponent was observed by Tong & Goldburg (1988). This variation is initially like a half-power law and is reminiscent of typical critical phenomena. Unfortunately, one cannot read too much into this analogy because of possible crossover effects relating to the size of the "turbulent system." Note that the system size, equal to the available scaling range L/η, is small at low Reynolds numbers, indicating that finite-size effects may be important. At high enough Reynolds numbers, the system size increases to levels where finite-size effects become unimportant. The principal effect of increasing the Reynolds number further is that the scaling range increases without affecting the dimension.

Conversely, at a fixed Reynolds number of order 2000, the laminar part of the jet close to the nozzle is circular in section with a dimension of 1. Far enough downstream, however, the jet becomes turbulent, and, as discussed already, the cross section there attains the value 1.36. Prasad & Sreenivasan (1990b) confirmed this expectation and showed that the dimension rises rapidly through the transition region (typically within a distance of about 4 nozzle diameters from the exit).

We must note the results of Redondo & Linden (1988), who show that the dimension of a density interface in stratified turbulence decreases with increase in Richardson number. Also, there are indications (Johnson 1989) that the dimension of the density interface in a turbulent boundary layer at Mach numbers of order 3 is about 1.2—substantially smaller than that in incompressible flows.

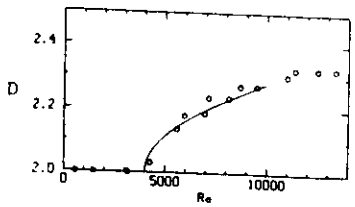

Figure 8 The dimension variation of a planar intersection of an isoconcentration surface as a function of Reynolds number in a temporally developing mixing layer (from Ramshankar 1989). The initial rise of the dimension can be fitted rather well by a half-power law, as shown.

3.3 *The Dimension in the* B*-Range*

For the typical jets and wakes examined by Prasad & Sreenivasan (1990b), the Batchelor scale is of order 4 μm. It is presently difficult to obtain such resolutions in planar cuts of any significant extent, and the only method appears to be line cuts invoking Taylor's hypothesis—in spite of its shortcomings discussed earlier. Sreenivasan & Prasad (1989) obtained such measurements by properly focusing a beam of light and obtaining the LIF trace as a function of time. Figure 9 shows the usual log-log plot for one-dimensional cuts through the interface. There are two distinct power-law regimes in each of the two ranges. As expected from earlier measurements in the K-range, the slope in the latter region is around -0.36, giving the expected dimension of 2.36. The B-region has a slope of about -0.75, giving a dimension of 2.75; the average slope from several realizations, including from jets, is 2.7 ± 0.03. These results are included in Table 1. The Schmidt-number dependence of these results is discussed in Section 3.6.2.

3.4 *The Dimension of the Vorticity Interface*

Corrsin (1943) discovered that unbounded turbulent flows possess at high Reynolds numbers the so-called vorticity interface, across which vorticity

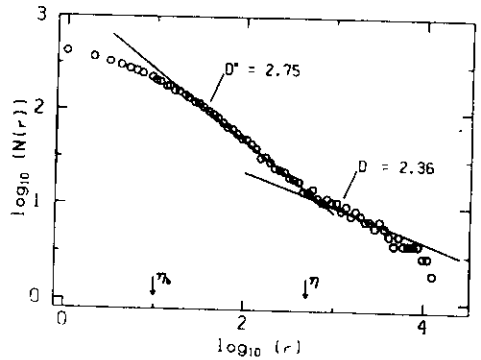

Figure 9 A typical log-log plot of the number $N(r)$ of line elements of size r containing the interface versus the box size r in the B-range. Measurements were made off-axis in the plane wake of a circular cylinder, 75 diameters downstream. The data are generated from single-point fluorescence measurements of the dye concentration, with a spatial resolution comparable to the Batchelor scale and ultrafast temporal response. The negative slopes of the straight parts yield, in the respective scaling regimes, the dimensions of line intersections with the interface. The interface dimension, corresponding to the lines drawn, is 2.36 in the K-range and 2.75 in the B-range. The substantial scatter in the K-range results from the fact that extremely fine resolution of the measurements necessitated the use of a signal length that could not capture many large scales. From Sreenivasan & Prasad (1989).

changes are rather sharp. This is in general different from the scalar interface. It has so far been impossible to study the vorticity interface in as much detail as the scalar interface. In particular, its fractal dimension has been measured only in line intersections (Fan 1988) using the streamwise component of vorticity and Taylor's hypothesis. Vorticity measurements were made with a small four-wire probe built with a modification of the original design of L. Kovasznay. As with scalar sections, a certain threshold on vorticity is set, and a box-counting algorithm is used on the intersections. The inset in Figure 10 shows the square of the vorticity signal and the threshold used for distinguishing the boundary-layer vorticity from background fluctuations and noise. The outer-layer intermittency is significant ($y/\delta = 0.9$, where δ is the boundary-layer thickness). The dimension from the log-log plot is about 2.37. [The threshold chosen in the figure (indicated by the arrow on the ordinate scale) suppresses more than just the background noise, but this does not appear to be critical. At worst, the correct interpretation of the dimension result is that it belongs to an isovorticity contour within the flow. Overall, however, conclusions on the fractal structure of the vorticity interface are more tentative than those for the scalar interface.]

3.5 *The Dimension of Atmospheric Cloud Boundaries*

Fractals appear in the literature on clouds, most simply because the boundary undulations are expected to be self-similar. The earliest dimension measurements for clouds and rain areas are due to Lovejoy (1982), who detected them, respectively, by infrared images from a geostationary satellite and by radar images. The rain areas belong to the tropical Atlantic region, and the cloud data covered the Indian Ocean within $\pm 30^\circ$ of longitude from the subsatellite point and $\pm 20^\circ$ of latitude from the equator. Both cumulus and cirrus clouds were included. The infrared images yield estimates of cloud-top temperatures, and so a threshold on the temperature was set to mark the boundary. Similarly, a threshold on the rain rate was used to define rain-area boundaries.

Lovejoy found that the cloud data obeyed the perimeter-area relation (2.5) for clouds with areas between approximately 1 and 10^6 km^2, and he deduced that the cloud perimeter has a fractal dimension of 1.35 ± 0.05. The scaling is remarkable--considering that the largest cloud extended from central Africa to southern India, a distance that is many times the scale height of the atmosphere.

A different situation from Lovejoy's was analyzed, again using (2.5), by Rys & Waldvogel (1986). They collected radar-echo data during severe convective storms and found that large clouds had a dimension of 1.36 ± 0.1, quite close to the value found by Lovejoy. However, small

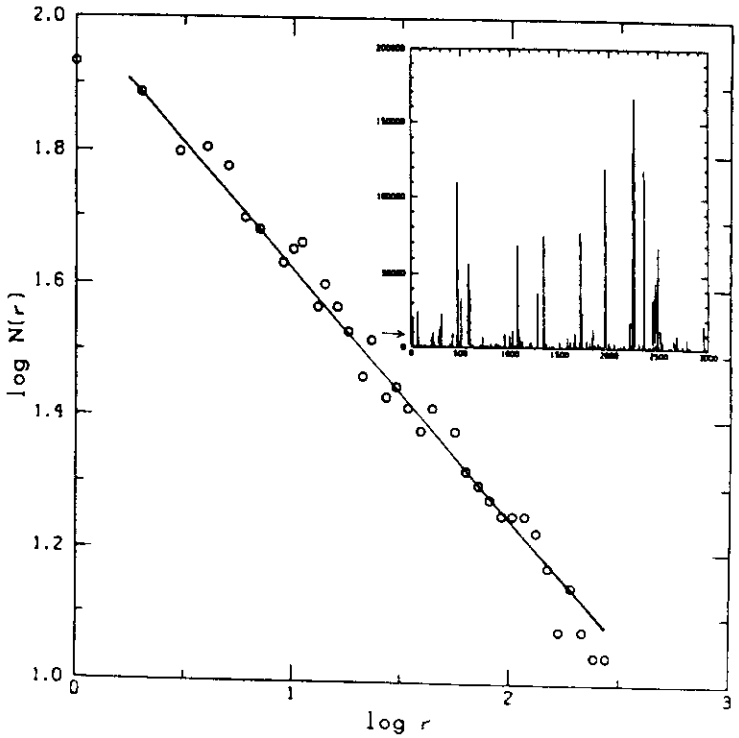

Figure 10 A typical log-log plot of the number $N(r)$ of line elements of size r containing the vorticity interface versus the box size r. The flow is a standard turbulent boundary layer developing on a flat wall. The momentum-thickness Reynolds number was about 2500, and the estimated resolution of the streamwise vorticity probe was 4η. The negative slope of the straight part, giving the fractal dimension of the interface in a one-dimensional intersection, is 0.37. The dimension from the additive law is 2.37, consistent with similar results from Sreenivasan & Meneveau (1986). The inset shows a segment of the squared-vorticity signal obtained from the probe. The log-log plot was generated by setting a threshold (indicated by the *arrow*) of 10^4 (in the units of the ordinate for the inset) on this signal and performing box counting on the set of intersection points. Taylor's hypothesis was used to interpret the signal as a one-dimensional cut (from Fan 1988).

clouds with the characteristic length [$=(\text{area})^{1/2}$ or $(\text{perimeter})^{1/D}$] smaller than about 3 km had a dimension close to unity. It was suggested that the low dimension of the smaller clouds was due to the strong vertical winds prevalent in thunderstorms. (For a similar effect on large clouds, pro-

portionately larger horizontal winds would be required.) The basic conclusion, then, is that fair-weather clouds as well as large clouds would have the same fractal dimension as the scalar interface, whereas clouds strongly affected by the mean wind would be smoother.

Finally, Prasad & Sreenivasan (1990b) examined the fractal dimension of boundaries in ground-based photographs of cumulus clouds obtained with the camera optic axis perpendicular to the ground; appropriate filters were used to eliminate background radiation. The box-counting method on the boundary of the cloud, determined by the threshold method, yielded a fractal dimension of 1.23 ± 0.03, which coincided with that measured for projection images in laboratory flows. Assuming the thick-section results from laboratory flows also hold for clouds, Prasad & Sreenivasan deduced that the dimension of boundaries in typical cumulus cloud sections would be 1.36; it follows from the additive law that the dimension of such cloud surfaces would be 2.36.

A very different approach is that due to Carter et al (1986), who use graphs of infrared emissions from clouds as a function of the angular distance at a fixed time to estimate fractal dimensions. They obtained dimensions of about 1.16 for midwave sections and 1.11 for longwave sections. As already stated, such graphs are self-affine and the dimension measurement is quite subtle.

Mention must now be made of the study by Lovejoy & Mandelbrot (1985), who emphasized the reconstruction of cloud patterns by use of fractal models. These authors proposed that a rain field is composed of self-similar pulses whose areas follow power-law distributions and within which the rain rate is chosen randomly. The resulting pictures look quite realistic. However, Lovejoy & Schertzer (1985) point out that clouds are quite stratified in the vertical direction, a fact that introduces self-affinity rather than self-similarity.

Such reconstructions for turbulent shear flows have not been attempted.

3.6 *An Interpretation of Dimension Results*

It has now been shown that the vorticity interfaces in several fully turbulent flows, as well as the scalar interface in the K-range, have a dimension of about 2.36 (Table 1). The apparent generality of this result must have a simple explanation. Sreenivasan et al (1989b) provided a heuristic argument relating the fractal dimension of surfaces to entrainment and mixing in turbulent flows, and they showed that simple considerations lead to predictions consistent with the measurements. The argument is the following: While the large structure in turbulence determines the precise amount of mixing, it is eventually the diffusive action at the molecular level that performs the actual mixing. This late stage adapts itself to

conditions set by the large-scale features of the flow. The main points are that the nonlinear dynamics of turbulence imparts fractallike properties to surfaces (see Section 3.2 for various cautionary notes), and that the result is a large increase in surface area. The diffusive flux across these surfaces follows the well-established Fick's law of diffusion and can be calculated easily. It is worth emphasizing that this picture implies neither that the role of large eddies is minimal nor that gradient transport as understood in turbulence closure is necessary or correct.

3.6.1 UNIT SCHMIDT NUMBER

The number of boxes $N(r)$ required to cover the surface and the corresponding area $S(r)$ at resolution r follow the relations

$$N \sim (r/L)^{-D}, \qquad S \sim (r/L)^{2-D}. \tag{3.1}$$

In all practical circumstances, the scale range over which these power laws hold is bounded by cutoffs on both ends. We have already shown that the outer cutoff occurs at scales comparable to the integral scale L of turbulence, and that the inner cutoff occurs at η. The existence of a finite inner cutoff means that as the surface area gets measured by covering it with increasingly finer elements, a point is reached beyond which convolutions of even finer scales no longer exist, and thus that the area will saturate (abruptly in an ideal situation) at the maximum value corresponding to the inner cutoff (Figure 11*a*). For the surfaces considered here, the situation at the outer cutoff is typically as shown, since these surfaces are roughly two dimensional when viewed at scales larger than L. (One thus has an interesting situation in which surfaces in turbulent flows look classical when observed at scales finer than the inner cutoff or at scales coarser than the outer cutoff but display scaling properties in the intermediate range.)

The true area S_t of a fractal surface with finite inner cutoff is given by the knowledge of the fractal dimension (which gives the slope in the self-similar regime of the line in Figure 11*a*) and of the inner and outer cutoffs (which truncate the power-law behavior). Thus,

$$S_t = S_0(\eta/L)^{2-D}, \tag{3.2}$$

where S_0 is the area measured with resolution L. Sreenivasan et al (1989b) argued that the gradients across the scalar interface are of order $\Delta C/\eta$, where ΔC is the maximum concentration difference in the flow, and showed that flux across the interface can be written as

$$\text{contaminant flux} = A\,\mathrm{Re}^{3(D-2)/4}. \tag{3.3}$$

Here Re is the characteristic Reynolds number, and the function A depends only on large-scale features. Since the amount of flux is determined by the

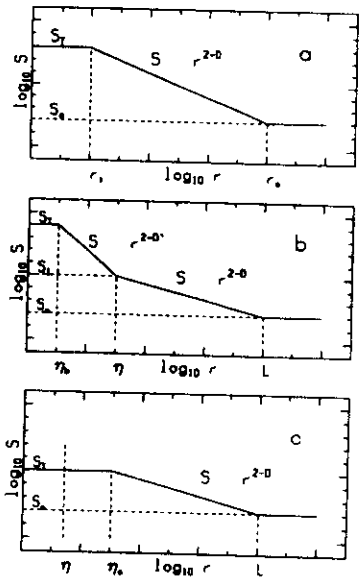

Figure 11 (*a*) Schematic variation of the area S of the scalar interface (Sc = 1) with respect to the scale of resolution r. The power-law behavior extends over a scale range that depends on the Reynolds number. In general, the inner cutoff occurs at the Kolmogorov scale η (or a small multiple of it), and the outer cutoff occurs at the integral scale L. The true area S_T of the surface is given by the saturation at the inner cutoff. In (*b*) are shown similar variations for the case Sc ≫ 1. The two scale-similar ranges in the K-range and the B-range are terminated as shown. The true area corresponds to that at the inner cutoff for the B-range, namely the Batchelor scale η_b. In (*c*) the case of Sc ≪ 1 is shown. The inner cutoff at the Corrsin-Obukhov scale η_c determines the true surface area (from Sreenivasan et al 1989b). The uppermost part of the figure also appears in a similar context in Gouldin (1988).

large scale, it must be independent of the Reynolds number. This is the so-called Reynolds-number similarity (e.g. Townsend 1956). It follows from (3.3) that $D = 7/3$, in rough agreement with experiments (Table 1). A similar argument by Gouldin (1988) yields the same result.

In obtaining this result, no allowance was made for possible spatial variations of normal concentration gradients along the interface, and thus the estimate must be treated as rough. Multifractal corrections (Sreenivasan et al 1989b, Meneveau & Sreenivasan 1990a), to be discussed in Section 6.1, show that the interface dimension is 2.36, in excellent agreement with measurements.

3.6.2 NONUNITY SCHMIDT NUMBERS Denoting the dimensions in the K- and the B-regions by D and D', respectively, the relation between the surface area and the resolution of measurement can be obtained (Figure 11*b*). If S_1 is the area measured with resolution η and S_1 is the true area measured with a resolution η_b, we have $S_1 = S_0(\eta/L)^{2-D}$ (as before) and can write

$$S_T = S_1(\eta_b/\eta)^{2-D'} = S_0(\eta/L)^{2-D}(\eta_b/\eta)^{2-D'}. \tag{3.4}$$

The estimate for the gradients is of order $\Delta C/\eta_b$, so that the result for the flux of a species with concentration difference ΔC is given by

$$\text{contaminant flux} = B\,\mathrm{Re}^{3(D-2)/4}\mathrm{Sc}^{0.5(D'-3)}, \tag{3.5}$$

where B is a function of large scales, independent of Reynolds and Schmidt numbers. Schmidt-number similarity [$\mathrm{Sc} \to \infty$, but $(\ln \mathrm{Sc})/\mathrm{Re}^{1/2} \ll 1$] requires that $D' = 3$. This means that convolutions of the interface on scales between η_b and η are space filling. The physical picture is shown in Figure 12. The convolutions in the K-range are self-similar, with a dimension of 2.36, but those in the B-range are much more pronounced; having a fractal dimension of 3, they essentially fill the space and render the effective thickness of the interface of order η even for high Schmidt numbers. Sreenivasan & Prasad (1989) have argued that the finite Schmidt-number corrections are of the form $D' = 3 - 2\ \ln(\ln \mathrm{Sc}^{1/2})/\ln \mathrm{Sc}$. In the limit of infinite Schmidt numbers, one gets $D' = 3$. For a Schmidt number of 1930, as for the fluorescing dye (Ware et al 1983), one finds that $D' = 2.65$, quite close to the measured average value of 2.7 (Table 1). Systematic coarse-graining arguments used by Meneveau & Sreenivasan (1990a) yield functions A and B that are within a factor of ~1.5 of experimentally determined values.

It should be mentioned that Vassilicos (1989) has calculated on the basis of a simple model the roll-off rate in the spectral density of a passive nondiffusive scalar. The roll-off rate is $D - 4$, where D is the dimension of the interface between regions where the scalar is unity and the regions where it is zero. Using $D = 7/3$ for the K-range, we get the spectral exponent of $-5/3$, whereas in the B-range a dimension of 3 for the interface

Figure 12 Schematic of the scalar interface when scales in the B-range are resolved (from Sreenivasan et al 1989b).

leads to the exponent of -1. These results are completely consistent with classical turbulence theories. Vassilicos has also shown that the dimension of the interface is a time-dependent quantity.

For $Sc \ll 1$, the inner cutoff occurs (Obukhov 1949, Corrsin 1951) at $\eta_c = Sc^{-3/4}\eta$, which is larger than η, and the only exponent is D (Figure 11*c*). The area is then $S_0(\eta_c/L)^{2-D}$ and the corresponding contaminant flux is $C\,Re^{3(D-7/3)/4}Sc^{3(D-7/3)/4}$, yielding, from Reynolds- and Schmidt-number similarities, $D = 7/3$ as before.

Clouds are high-Reynolds-number objects, and the fact that their surfaces have the same fractal dimension as interfaces in ordinary turbulent flows may be due to very similar reasons. Hentschel & Procaccia (1984) provided a different explanation based on their theory of relative turbulent diffusion: Clouds are considered to be scalar-marked regions within which the contaminant spreads by turbulent diffusion. Briefly, these authors wrote an evolution equation for the two-point structure functions describing all their initial values, relating them to the dimension of the boundary. The result is that $D = 7/3 + \mu/6$, where μ is the intermittency exponent (which we briefly describe in Section 6.1). Using a value of 0.26 for μ, we obtain a fractal dimension of 2.37, in excellent agreement with measurements as well as with the above argument. We do not discuss the Hentschel-Procaccia theory in detail here, because it is quite involved and partly because two crucial assumptions of the theory have been questioned by Ball & Kingdon (1988; see also Vassilicos 1989). However, Ball & Kingdon obtained the same final result as Hentschel & Procaccia because of the cancelling effect of the two assumptions in question.

4. FRACTAL DIMENSION OF FLAME SURFACES

In some special circumstances, especially for premixed flames (see, for example, Pope 1987), reactions in turbulent flames are confined to thin sheets called flamelets. There is, therefore, much interest in a theoretical framework based on the surface area of flamelets. Early attempts concentrated on treating them essentially as wrinkled laminar flames, but, as Libby & Williams (1976) point out, a treatment of flamelets by wrinkling laminar flames in ad hoc ways is not adequate. For nonpremixed flames, Libby (1974) conjectured that the flame sheet is similar in character to the interface. From our previous discussion, this suggests that fractal models may be appropriate for flames also.

Gouldin (1987) realized the value of fractal geometry as a potential tool for describing flamelets in turbulent-combustion problems. There now exists a sizable literature on fractal-dimension measurements in premixed and nonpremixed flames (Gouldin et al 1988, Strahle & Jagoda 1988, Murayama & Takeno 1988, Goix et al 1989, Mantzaras et al 1989a,b, Chen & Goss 1989, North & Santavicca 1990). There has been considerable work in the direction of building fractal-based models for turbulent combustion (Gouldin 1987, Gouldin et al 1989, Santavicca et al 1990, Chin et al 1990a,b).

A common scheme for obtaining two-dimensional slices of the flame is called laser tomography by the combustion community. It consists of introducing scattering particles (for example, titanium dioxide particles) into the flame and measuring the Mie scattering intensities in slices of the flow. As with scalar interfaces, the boundary is defined in a suitable way, and its dimension is measured. Co-dimension methods, variants of the boundary-length method, and box-counting methods all have been used. Temporal scattering data obtained by "point" probes, interpreted as one-dimensional cuts, have also been used. The validity of the additive law has not been studied in as much detail for flames as for scalar interfaces, but it is implied in much of the work. In further discussion, we too shall assume its validity.

The work of Gouldin et al (1988) for the nonpremixed case (jet Reynolds numbers between 4800 and 10,400) has yielded a dimension of 2.36 ± 0.05, while that of Mantzaras et al (1989a,b) for premixed flames in internal combustion engines has resulted in a value of $2.36 \pm 3\%$. These results are in good agreement with the scalar-interface dimension, but other investigators have obtained different results. For example, Chen & Goss (1989) quoted a value of 2.31 ± 0.07 for diffusion flames, Murayama & Takeno (1988) (who studied tomograms of flamelet surfaces in two orthogonal sections) obtained an average dimension of 2.26 for a premixed methane-air flame, and Goix et al (1989) measured a dimension of 2.2 for similar types of flames; Gouldin et al (1988) measured a value as low as 2.1 for the flamelet surface in their premixed methane-air V-flame.

Apart from the fact that it is inherently more difficult to make dimension measurements in flames, the following comments may shed some light on the variability in the data. First, the high flame temperatures tend to depress Reynolds numbers to low values displaying Reynolds-number sensitivity (Section 3.2). For example, the integral-scale Reynolds number was of the order of 25 in the flames of Goix et al and in the premixed flames of Gouldin et al. Second, measurements have often been made in the vicinity of the flame holder, where the fractal dimension (as discussed in Section 3) continues to increase with downstream distance; for example, in the Goix et al study the value was not saturated, even at their last measuring station. Under the circumstances, the asymptotic value obtained for the scalar interfaces can perhaps be seen only if turbulence

levels in the oncoming stream are high enough to maintain the flow fully turbulent at relatively low Reynolds numbers. High turbulence levels tend to fragment the flamelet surface, but this situation does not present any problems in either the measurement or the interpretation of the dimension. Dimension measurements do indeed show strong dependence on turbulence level (Figure 13), asymptotically approaching ~ 2.36 when the turbulence level is high. Finally, the laser sheets used for obtaining tomographic sections are not always thin enough by the criterion discussed in Section 3.2: It is clear from the thick-section measurements of Prasad & Sreenivasan (1990b) that the resulting dimension is likely to be smaller than the thin-section value. Some reduction in the dimension value results also if the flame image is smeared—as appears to be the case in some measurements because the laser pulse is not narrow enough to freeze the flame on its smallest scale.

On balance, it appears that flame surfaces in premixed as well as diffusion flames have a dimension close to that of the scalar and vorticity interfaces in isothermal flows, *provided* that distances far downstream of flame holders are considered and the oncoming stream is maintained highly turbulent. This conclusion should not surprise us for nonpremixed flames, where the flame surface is very similar to the interface of a passive scalar. Premixed flames, on the other hand, are generically different, but it is possible that at high enough turbulence levels the flamelet surface approaches the properties of a scalar interface (see, for example, Mantzaras et al 1989b). We have an interesting and potentially useful conclusion here—if the observation is indeed true.

As already noted, the fractal concept has been used for predictive purposes in combustion. Following an earlier proposal due to Damköhler (1940) that the flame speed V is proportional to its surface area S, Gouldin

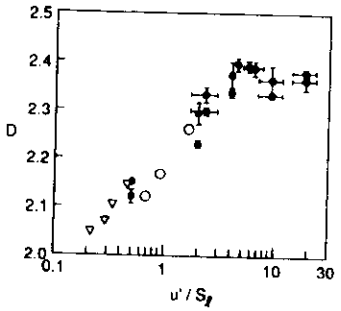

Figure 13 The variation of the fractal dimension in premixed flames as a function of the turbulence level (normalized by the laminar flame speed S_l). The initial increase appears exponential to a good approximation, and the asymptotic value is comparable to that for scalar interfaces in isothermal flows. *Filled circles* are from Mantzaras et al (1989a,b), *triangles* from North & Santavicca (1990), and *open circles* from Murayama & Takeno (1988).

(1987) conjectured that $V_t/V_l = S_i/S_o$, where the subscripts t and l refer to the turbulent and laminar conditions, respectively, and subscripts i and o refer, respectively, to surface areas measured at inner and outer cutoffs, as discussed in Section 3.6. The outcome of this hypothesis has been shown to be reasonable by Gouldin (1987) and Mantzaras et al (1989a). Another application of the fractal concept has been in the chemical closure. Gouldin et al (1988) proposed a model that expresses the fuel combustion rate in terms, among other things, of the fractal dimension of flamelets. This model was combined with a second-order transport model with conditional statistics, and numerical calculations were performed. The results were deemed satisfactory by the authors. Santavicca et al (1990) have used fractal-based models to predict turbulent-flame kernel growth and concluded that the predictions are in good agreement with measurements. Chin et al (1990a,b) used similar ideas in modeling turbulence effects on combustion in piston engines and concluded that they offer promising tools in engineering design and development. However, it must be borne in mind that these various favorable conclusions also involve turbulence modeling in some form.

Finally, we should remark on the inner and outer cutoffs of the scaling observed in flames. The outer cutoff, as in scalar and vorticity interfaces, extends to the integral scale and perhaps even beyond. The precise determination of the inner cutoff has, however, remained elusive because of measurement difficulties. Mantzaras et al (1989b) have described these difficulties. Gouldin noted that the flamelet propagation would increase the inner cutoff scale and drive it toward the outer scale in the limit of vanishing turbulence level. For large turbulence levels, he assumed the inner-cutoff scale to be of the order of the Kolmogorov scale. Goix et al (1989), as well as Murayama & Takeno (1988), stated that it is of the order of the flame thickness. For intermediate turbulence levels, Peters (1986) noted that the intrinsic lower bound on scales in the multiply connected flamelet surface in premixed combustion is on the order of the Gibson scale. (The Gibson scale is defined by the condition that its characteristic velocity must equal the flame speed.) Experiments do not support this suggestion unequivocally: For example, Gouldin (1987) implied that it was contradicted, whereas Murayama & Takeno (1988) explicitly stated so. North & Santavicca (1990) found that the inner cutoff was smaller than the Gibson scale. F. V. Bracco (private communication) has noted that Peters' suggestion about the Gibson scale is self-consistent if its use is limited to cases where the Kolmogorov scale is larger than the flame thickness and the root-mean-square turbulent fluctuation is substantially larger than the laminar-flame speed.

5. MULTIFRACTALS

5.1 *Introduction*

All objects considered previously have been identified by specifying that some measure distributed on them is uniform: For example, the concentration on an isoconcentration contour is by construction the same everywhere. A description of such sets is then the same as that of the measure living on them. On the other hand, consider an instantaneous realization of the scalar dissipation rate $\chi \sim [\text{grad } C]^2$; the set here is the space marked by the scalar, and the measure living on it is χ. As shown in Figures 14*a* (see color insert) and 14*b*, this measure is highly spiky in nature. The geometry of the set on which χ is distributed is thus only a part of the picture, and a more detailed machinery is necessary to describe χ itself. As a second example, consider Figure 15, which shows one-dimensional sections of a component of energy dissipation in a laboratory flow at moderate Reynolds number and in the atmosphere at higher Reynolds number. It is again clear that the distribution displays strong nonuniformities. Such highly intermittent measures cannot be described efficiently by the usual moment methods. In particular, if a measure has a Gaussian distribution, its mean and variance describe the process completely; for others close to Gaussian, a few low-order moments contain most of the information. For measures of the type shown in Figures 14 and 15, on the other hand, the first few moments give little clue to their nature.

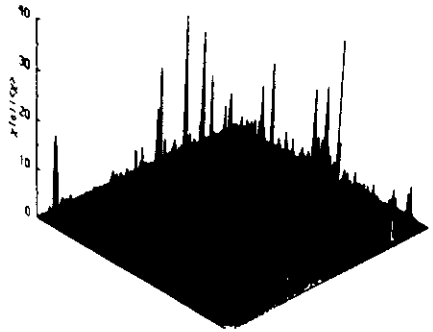

Figure 14b The quantity χ is plotted for a small rectangular area in a planar section of a jet. All three components of χ have been measured here; the third component has been estimated by differencing concentration levels between two parallel planes separated by about 4η. This figure illustrates quantitatively the spatial intermittency of the dissipation field (from Prasad & Sreenivasan 1990a).

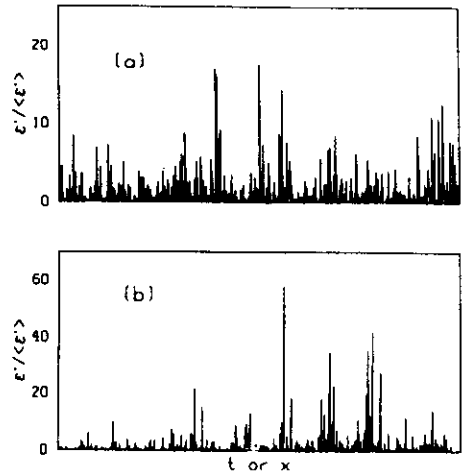

Figure 15 Two typical signals $\varepsilon' = (du/dt)^2$, serving as the surrogate of the energy dissipation rate, are plotted here upon normalizing by their mean values. Graph (*a*) was obtained in a standard flat-plate laboratory boundary layer at a momentum-thickness Reynolds number of 3600. The measurement station was 0.2δ, where δ is the boundary-layer thickness (~ 4 cm). The microscale Reynolds number there was 110. Graph (*b*) was obtained in the atmospheric surface layer at a height of about 18 m above the ground. The mean wind speed was about 6 m s^{-1}, and the estimated microscale Reynolds number was 1800. The increased intermittency at the higher Reynolds number is obvious. This intermittency, representing the fact that there is a definite limit to small-scale mixing, is believed to be an important feature of turbulence (from Meneveau & Sreenivasan 1990b).

The description of such intermittent measures belongs to the domain of multifractals. Essentially, multifractals are built up by a procedure (which is often rather simple) that proceeds from one scale (the parent scale) to the next smaller ones (the offsprings) in such a way that the measure (for example, the rate of energy dissipation) contained in the parent scale is unequally divided among its offsprings. When this procedure repeats many times, the measure on the offsprings at each successively higher generation will become increasingly uneven. Because the measure on an arbitrary offspring at a given generation level is determined by the product of the multipliers (i.e. numbers characterizing the unequal division of the measure) of all its forefathers, a multifractal can be associated with a multiplicative process (or a cascade). If the basic rule determining the unequal division from a parent scale to its offsprings is independent of the

generation level, one expects certain scale-similar properties. Our primary concerns are to determine whether the multifractal scaling indeed occurs for intermittent turbulence and to deduce the multiplicative process leading to such a scaling.

A physical picture leading to intermittent distributions, dating back to Obukhov (1962) and Kolmogorov (1962), visualizes kinetic energy flux to small scales as a self-similar cascade. These authors proposed log-normal distributions for the probability density of such quantities. Novikov (1970), Orszag (1970), and Mandelbrot (1972) have shown that log-normal distributions have inherent problems. A different type of intermittency model was proposed by Novikov & Stewart (1964). For critical assessments of these features, see Kraichnan (1974), Levich (1987), and Nelkin (1989), as well as Chorin (1988a). Mandelbrot (1974) introduced a general cascade model using notions of fractal geometry. The physical and geometrical implications of this model were analyzed by Frisch et al (1978), who coined for their specific version the name β-model. Frisch & Parisi (1985) introduced the idea that intermittent distributions can be described in terms of singularities of varying strength, all lying on interwoven sets of different fractal dimensions, and coined the name multifractal. They related such a description to the hierarchy of moment exponents originally proposed by Mandelbrot (1974). Benzi et al (1984) presented the random β-model. Hentschel & Procaccia (1983) introduced a hierarchy of generalized dimensions D_q, and Halsey et al (1986) introduced $f(\alpha)$ for the fractal dimensions of sets of singularities characterizing multifractals. Mandelbrot (1989b) further clarified some properties of $f(\alpha)$ in terms of his earlier work.

The usual reason for expecting multiplicative processes in physical space to hold for turbulence is Richardson's (1922) picture of large eddies of turbulence sequentially splitting into smaller ones to which the energy is believed to flow. There is no real evidence, however, that this actually happens. What may actually occur is a process of stretching (and tilting) and folding a blob of fluid elements into successively thinner structures -- known as the horseshoe process in dynamical systems. (For an argument that stretching and folding must coexist, see Chorin 1988b.) The overall isotropy and simplicity of the breakdown of blobs are absent in this process, and its precise relation to the Richardson cascade remains to be clarified. It is, nevertheless, a multiplicative process in that the thickness and density of each piece are products of successive multipliers. To each piece is associated a characteristic length scale $r(n)$, n being the generation number, that is given by the product of n numbers (to be called length multipliers l_j), each of which is the ratio of consecutive length scales. In other words,

$$r(n) = r(0)\prod_{j=1}^{n} r(j)/r(j-1) = r(0)\prod_{j=1}^{n} l_j. \tag{5.1}$$

The total energy dissipation E_r (or the scalar dissipation X_r) in a certain piece Ω of size r is the integral of $\varepsilon(\mathbf{x})$ [or $\chi(\mathbf{x})$] over the piece Ω, i.e.

$$E_r = \int \varepsilon(\mathbf{x})\, d^3x \quad \left(\text{or} \quad X_r = \int \chi(\mathbf{x})\, d^3x\right). \tag{5.2}$$

Analogous to the situation with length scales, the total dissipation on a certain piece of size $r(n)$ is given by the product of n numbers (to be called measure multipliers M_j), each of which is the ratio of consecutive measures. For the energy dissipation,

$$E_{r(n)} = E_{r(0)}\prod_{j=1}^{n} E_{r(j)}/E_{r(j-1)} = E_{r(0)}\prod_{j=1}^{n} M_j. \tag{5.3}$$

When a piece Ω breaks up into smaller ones, each smaller piece can be thought of as receiving a fraction of E_r or X_r. These fractions may or may not add to unity, depending on whether or not the cascade is conservative.

For deterministic multiplicative processes, the multipliers l_j and M_j are fixed numbers. For turbulence, it is likely that they will be random variables with some probability distribution. If the distribution function does not depend on the level j, self-similarity will appear.

5.2 *Characterization of Multifractals by the Singularity Spectrum and Generalized Dimensions*

In the standard multifractal formalism, one assumes that at each stage the length splits into equal pieces, but that the measure gets distributed unequally. Since intermittency can be caused by the unequal splitting of either length or measure multipliers or both, none of which is in general known for turbulence, the best way to proceed is not clear. However, for deterministic multifractals, Chhabra et al (1989a) have shown that one can do as well by assuming unequal splitting of lengths as by assuming unequal splitting of measures. Therefore, one covers the set (line, area, or volume) by equal boxes of size r and writes the integrated measure in the box as

$$E_r/E_I \sim (r/L)^{\alpha} \quad \text{or} \quad \varepsilon_r/\varepsilon_L \sim (r/L)^{\alpha - d}. \tag{5.4}$$

Here, α is an exponent that depends on the position of the box, reflecting the fact that multifractal scaling is only local. Writing the integrated measure in this form emphasizes that different values of α are associated with different strengths of singularities (in the sense that $\varepsilon_r \to \infty$ as $r \to 0$ for all $\alpha < d$), with smaller α values corresponding to larger peaks. All $\alpha > d$ correspond to regular regions (in which ε_r can be expanded by Taylor

series). One now assumes that the entire measure consists of an infinity of iso-α sets intertwined together. Some appreciation for this fact can be had from Figure 14*a*, where (crudely speaking) one can assign different α's to the different colors used in the figure. Multifractal analysis aims to obtain the so-called singularity spectrum, or the fractal dimension $f(\alpha)$ of each iso-α set. One writes, in analogy to self-similar fractals (Section 2.2), the number of boxes of size r that assume α values within a band of width $d\alpha$ as

$$N(\alpha)\,d\alpha \sim \rho(\alpha)(r/L)^{-f(\alpha)}\,d\alpha. \tag{5.5}$$

Here $\rho(\alpha)$ is some α-dependent prefactor. In cascades, N is also the total number of pieces resulting from the multiplicative process when they have reached a scale r. It is assumed that the prefactor does not depend on r, this being true only in the limit of infinite scaling. In practice, there are logarithmic correction terms (Van de Water & Schram 1988, Meneveau & Sreenivasan 1989), with which we do not concern ourselves here.

Another way of characterizing a multiplicative measure is via moment exponents $\tau(q)$ defined through the relation

$$\sum E_r^q \sim E_L^q (r/L)^{\tau(q)}. \tag{5.6}$$

In different notations, Novikov (1969) and Mandelbrot (1974) introduced these exponents. In (5.6), q is a real number: When $q > 0$, the sum on the left-hand side gets its major contribution from peaks that get larger as q is increased, whereas when $q < 0$, increasingly more negative q's correspond to increasingly smaller intensities. Thus q can be considered an amplifier that can be tuned to accentuate peaks of a certain size, with $\tau(q)$ representing the appropriate scaling exponent. One can also define (Hentschel & Procaccia 1983) the generalized dimensions D_q as

$$D_q = \tau(q)/(q-1). \tag{5.7}$$

Hentschel & Procaccia (1983) showed that D_0 corresponds to the usual fractal dimension of the support of the measure, D_1 to the information dimension, and D_2 to the correlation dimension. In general, D_q is the dimension of a set that, when used to intersect the original measure, produces divergence of moments of order q (Mandelbrot 1989b).

The representations (f, α) and (D_q, q) are the first level of information about multifractals and are equivalent. Roughly speaking, they characterize the strengths of various singularlike regions and the dimensions of sets on which each of them is distributed. Following Frisch & Parisi (1985) and Halsey et al (1986), one can relate the exponents D_q, α, and $f(\alpha)$ through the Legendre-transform relations

$$f[\alpha(q)] = q\alpha(q) - (q-1)D_q, \qquad \alpha(q) = d/dq[(q-1)D_q], \tag{5.8}$$

with the condition that $f'(\alpha) < 0$ and $\partial f(\alpha)/\partial\alpha = q$. The Legendre transforms replace the local value of the function $\tau = (q-1)D_q$ by its slope $\alpha(q)$ and its intercept $f[\alpha(q)]$. When $\tau(q)$ is discontinuous, the relation (5.8) needs suitable modification.

Two cautionary remarks should be made. First, $f(\alpha)$ relates to the scaling behavior of $N(\alpha)$ only when α is defined by (5.4) with the same resolution used in the definition of $N(\alpha)$: One cannot use the measure at a fixed resolution, say $r = \eta$, and use box counting to calculate $f(\alpha)$. Second, Mandelbrot (1984, 1989b) and Cates & Witten (1987) have pointed out that the interpretation of $f(\alpha)$ as the dimension of the iso-α set is not always correct. For example, for processes whose multipliers are randomly distributed according to a smooth function that goes to zero at the tails, there will always be some parts of the measure that occur extremely rarely provided the sample is large enough. Instead of focusing on the number of iso-α boxes, one considers the probability $\Pi(\alpha)\,d\alpha$ of encountering values of α in a band $d\alpha$. This can be written as $(r/L)^{d-f(\alpha)}\,d\alpha$ from the fact that $\Pi = N/N_0$, where N_0 is the total number of boxes containing the measure given [according to (2.2)] by $(r/L)^{-d}$ or $(r/L)^{-D_0}$, depending on whether the measure fills the entire space or has a support with dimension D_0. In this view, $d - f(\alpha)$ is simply a scaling exponent.

The part of the $f(\alpha)$ curve in which both f and α are positive has been designated by Mandelbrot (1989b) as the manifest part. Here, the usual interpretation of $f(\alpha)$ holds. The part with $f < 0$ but $\alpha > 0$ has been called the latent part, while that with $\alpha < 0$ has been called the virtual part. Depending on the details of the distribution of multipliers, only one or two of these parts could form the entire $f(\alpha)$ curve. As already mentioned, the latent and virtual parts, if they exist, contain information on some rare events whose contributions to low-order moments are minimal. However, they are crucial to identifying the dynamics, in that they lie outside the jurisdiction of the central-limit theorem and are specific to the process (see also Sections 6.4, 6.5). These are also the events that are hard to quantify in experiment unless one takes many samples.

Finally, we should note that the multipliers, which are the analogues of the generator in deterministic fractals (Section 2.2), correspond in a rough sense to the scaling function (Feigenbaum 1978) in dynamical systems.

5.3 *Measurement of the Multifractal Spectrum*

5.3.1 GENERALIZED DIMENSIONS AND LEGENDRE TRANSFORMS This method consists of using Equations (5.6)–(5.8). Usually one does not exactly

know the prefactors in (5.6), but they can be eliminated by taking ratios at two different scales r. The generalization of this procedure is to use many different scales and generate log-log plots whose slope (if there is a linear region) will be the exponent sought.

In many applications one does not know the measure at different levels of the cascade but only at scales corresponding to the last cascade step. In general, one also does not know the size and exact position of the pieces resulting from the original multiplicative process. It turns out that it is possible to use boxes of sizes and positions different from the "natural partition," and, for a process that has progressed through many steps of the cascade, the results will be unaffected (except for the appearance of oscillations and fluctuations). Some errors do occur in box counting when the partitioning is incorrect and box sizes are large; their precise estimates, however, depend on the multifractal. For details, see Chhabra & Sreenivasan (1990a).

The main point is that the multifractal formalism is applicable to real measurements for which the measure at a single cascade step (usually at the inner cutoff) is available. This situation is very similar to that for self-similar fractal sets whose dimension can be measured by examining them at a fixed level of evolution by varying the resolution. The difference, however, is that we must additionally consider the *intensity* or *density* with varying degrees of resolution.

5.3.2 DIRECT METHODS OF DETERMINING THE $f(\alpha)$ CURVE One could obtain α and $f(\alpha)$ directly from definitions (5.4) and (5.5). However, by naively taking logarithms, one is left with adjustable constants due to the presence of unknown prefactors. Arnéodo et al (1987) assumed that these prefactors were constants independent of α or q and determined them by numerical fits based on data from three different boxes. It is much better to consider different length scales and obtain exponents from regression plots (Meneveau & Sreenivasan 1989). The convergence in either method is rather slow in the scaling range.

One can use to advantage the *formal* connection that exists between multifractals and the thermodynamics of statistical mechanical systems (Feigenbaum et al 1986, Feigenbaum 1987a,b; for a different view, see McCauley 1989). The natural connection to be made here (Chhabra & Jensen 1989, Chhabra et al 1989a, Mandelbrot 1989b) is the following. If we define an energy $\mathbf{E}_r = -\log[E_r/E_t]$, (5.6) gives the partition function for the box size r, from which, comparing standard thermodynamic relations with (5.8), one can see that f is proportional to the entropy and α to the internal energy, with τ and q as the analogues of the free energy and inverse temperature, respectively. Chhabra & Jensen also recognized,

on the basis of a theorem by Eggleston (1949) that itself uses Shannon's information theory (see, for example, Billingsley 1965), that the entropy is simply related to the Hausdorff dimension of the measure-theoretic support of the measure. In the thermodynamic view, the scaling ratio L/η is the size of the system, and the lack of convergence discussed earlier simply reflects finite-size effects. In canonical methods in statistical mechanics, one circumvents this problem by Boltzmann weighting. In effect, Chhabra & Jensen's method constructs a one-parameter family of normalized measures $\nu(q,r) = [E_r]^q/\sum[E_r]^q$, where E_r is the measure in a box of size r and the summation in the denominator extends over all boxes of size r. As in the definition of the generalized dimension, the parameter q provides a microscope for exploring different strengths of the measure: For $q > 1$, ν amplifies the more singular regions, whereas for $q < 1$, it accentuates the less singular regions. For $q = 1$, ν simply replicates the original measure. Then the Hausdorff dimension of the measure-theoretic support of $\nu(q)$ defines $f(q)$, whereas the singularity strength $\alpha = \ln[E_r]/\ln r$ is calculated by its average with Boltzmann weights. Therefore, one has f and α as implicit functions of the parameter q:

$$f(q) = \sum \nu(q) \ln \nu(q)/\ln r, \qquad \alpha(q) = \sum \nu(q) \ln E_r/\ln r. \tag{5.9}$$

Chhabra & Jensen (1989) and Chhabra et al (1989b) have established that this method works well both for dynamical systems and for turbulence and solves the problem of convergence.

5.3.3 THE MULTIPLIER METHOD Finally, it is possible to examine any two successive steps of the cascade and construct the multiplier distribution. In practice, one can perform suitable box averaging in the right scale range and determine the multipliers as ratios of the measure in the parent box to those of its offsprings. For a binary process, Mandelbrot (1989b) shows that

$$\log_2 \langle M^q \rangle = -d - \tau(q). \tag{5.10}$$

The rest of the quantities follow simply.

Chhabra & Sreenivasan (1990a,b) have pointed out that the multiplier method can be superior to the box-counting method. Its superiority is easy to establish when one knows the proper partitioning of the measure, but it is not easily demonstrable otherwise—except in the limit of infinite steps of the cascade. Further, an advantage of the multiplier method is that it puts to explicit use the existence of invariant level-to-level information and performs averaging both over boxes at any given level (as in the box-counting methods) and over boxes at different levels. For high-Reynolds-

number flows, this is perhaps the only practical method for computing the latent part of the $f(\alpha)$ curve.

6. MULTIFRACTAL SPECTRA IN TURBULENCE: EXPERIMENTAL RESULTS AND INTERPRETATION

The $f(\alpha)$ curve has been measured for several positive-definite quantities characterizing small-scale motion. For the energy dissipation, see Meneveau & Sreenivasan (1987a, 1990b); for the scalar dissipation rate, see Prasad et al (1988); for the squared and absolute vorticity, see Fan (1988) and Meneveau et al (1990); and for the absolute value of the Reynolds stress in the boundary layer, see Kailasnath (1988). We particularly invite the reader's attention to Meneveau & Sreenivasan (1990b) for a detailed discussion of the measurement techniques, signal/noise estimates, ambiguities in determining scaling regimes and exponents, etc. Several of these multifractal spectra have also been obtained from the NASA Ames Research Center data base by means of direct numerical solution of the Navier-Stokes equations for a channel flow (Dean & Keefe 1988).

6.1 *The Energy Dissipation Rate, or the Energy Flux in the Inertial Range*

The flux of kinetic energy is envisioned to proceed from large to small scales until the dissipation scale is reached. According to conventional thinking, its manifestation at this final step of the cascade is the energy dissipation rate, which is the measure of interest to us here. By the measurement of the final product of the cascade and its scaling in the inertial range, it is believed that one can actually determine the inertial-range properties relevant to the energy flux. This is justified below.

Since the measurement of the dissipation field in three-dimensional space has not been possible so far, one is constrained to making measurements in a plane or along a line. As discussed in Section 2.2, much information about the ubiquitous aspects of three-dimensional processes can be gained from typical lower dimensional intersections. This, however, is not true for events that occur rarely—say, less often than once per typical sample. Such events can be captured only by taking many one-dimensional cuts (Mandelbrot 1974) or by going very deep in the cascade level. Even the one-dimensional cuts studied so far have been of one component of the energy dissipation and invoke the frozen-flow hypothesis. The limitations of these approximations are not completely understood, but the following information may be useful. Prasad & Sreenivasan (1990a) have measured all three components of the scalar dissipation χ and have shown that the scaling of any one component is the same as that of the sum (although in several other respects the individual components differ from each other as well as from the sum). Whether this is true also of the energy dissipation is unclear, especially because ε contains cross-derivative terms while χ does not. Sreenivasan et al (1989a) have shown that, with qualifications similar to those mentioned in Section 3, Taylor's hypothesis is not unreasonable. In any case, in all measurements to follow in this section, the real energy dissipation rate is represented by its surrogate $\varepsilon' = (du/dt)^2$, where u is the fluctuating velocity in the streamwise direction. For convenience, the prime is dropped henceforth. All measurements have been made in fully turbulent parts of the various flows (i.e. the effects of outer intermittency have not been included).

Meneveau & Sreenivasan (1987a) obtained the first multifractal measurements of ε and followed them up with some analysis. They measured ε in a variety of shear flows and obtained D_q's for samples of order 10 integral scales. Each sample possessed a sizable scaling range (see Figure 16) spanning almost the entire range between L and η. The slopes, however, varied from one sample to another. For any given sample, the D_q's vary smoothly with q and, from sample to sample, do not intersect except at $q = 0$. A sample that has larger D_q for $q < 0$ also has smaller D_q for $q > 0$. Even more significantly, the fluctuations in f and α are highly correlated. Typical histograms of the fluctuating D_q's for some selected q's are presented by Meneveau & Sreenivasan (1987a). The spread of fluctuations was found to be larger than the uncertainty in log-log fits. These fluctuations are believed to be of fundamental importance, and their possible source is discussed in Section 6.5.

Meneveau & Sreenivasan calculated averages of the D_q exponents for a given q and obtained a smooth curve. Upon using (5.8), they obtained the $f(\alpha)$ curve. Such curves were the same (to within experimental accuracy) for all flows examined—leading to the claim of universality of small-scale motion. Alternatively, one can obtain the $f(\alpha)$ curve for each of the D_q curves and perform the averaging on the resulting $f(\alpha)$'s. This is not different from the previous average.

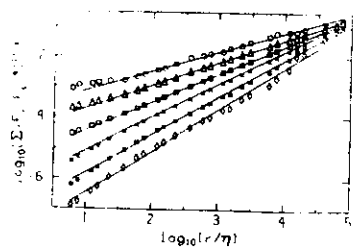

Figure 16 Typical log-log plots of $(\Sigma E_i)^{1/q}$ versus r for the dissipation field measured in the surface layer of the atmosphere for the conditions as in Figure 15*b*. E_i in the ordinate is normalized by the total measure E_t in the signal, and the box size is normalized by the estimated Kolmogorov scale η. Linear regions in these plots give the generalized dimensions. From *top* to *bottom*: $q = 4, 2, 0.6, -0.6, 2$, and 4 (from Meneveau & Sreenivasan 1990b).

On the other hand, one can also compute multifractal parameters from a supersample, or very long record of many thousands of integral scales, and eliminate fluctuations. When this was done, Meneveau & Sreenivasan (1990b) found that the results agreed well with the ensemble-averaged data in the manifest part of $f(\alpha)$—the two averages need not in principle give the same result—but two new features appeared. The first of these concerns the negative $f(\alpha)$'s. Recall, following Mandelbrot (1989b), that $f(\alpha)$ is related to the log-probability of events of specified singularity strength, and that an event occurring only once every sample yields an $f(\alpha)$ of exactly zero. It is then clear that negative $f(\alpha)$'s can result if an event occurs less often than once every *typical* sample. The observed sample-to-sample fluctuations automatically suggest that there is one strongest event and one weakest event that would dictate the extremes in the supersample and would lead, by virtue of their extreme rarity, to negative $f(\alpha)$. Thus, averaging over a supersample would eliminate fluctuations and unveil the latent $f(\alpha)$ presumed to have been present all along, hidden only by the artifact of ensemble averaging. Note that the negative parts correspond to one-dimensional cuts only. The accuracy of extreme tails of $f(\alpha)$ is still unclear, and so it is difficult to say with certainty whether the negative $f(\alpha)$ occurs in the three-dimensional process itself. For the moment, the issue remains unresolved.

However, supersampling degrades the scaling range from being approximately between L and η to a smaller subrange, roughly equal to the classical inertial subrange. The reasons for this are not completely understood, but it is believed that at least one of the reasons is the fluctuations we have mentioned earlier; another is that we are examining an essentially three-dimensional process in one-dimensional intersections. Whatever the reasons, supersampling makes it difficult to identify scaling in laboratory flows for which the available range ($=L/\eta$) is of order 200–300. This was the reason that Meneveau & Sreenivasan (1987a) restricted their attention to segments of order $10L$.

The $f(\alpha)$ curve for the energy dissipation is given in Figure 17. This has been obtained using 10^7 points and by considering the scaling in the inertial range, and its convergence—at least for a large part of the curve—has been established (Meneveau & Sreenivasan 1990b). The part of the curve above the arrow mark was obtained by direct evaluation of experimental data, whereas that below was obtained via a careful extrapolation of the histograms of log E_r. More recent work using the multiplier method is in agreement with these results, including the extrapolated part of the curve (Chhabra & Sreenivasan 1990b). Some salient features of the curve are the minimum α corresponding to the largest singularity in the distribution of ε, the maximum α corresponding to its least intense regions, the maximum

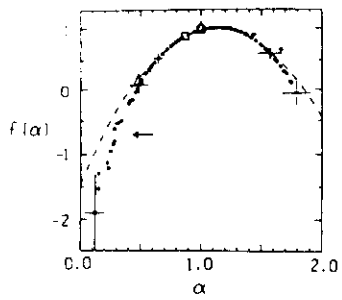

Figure 17 The $f(\alpha)$ curve for one-dimensional cuts of ε computed from generalized dimensions (*small circles* and *error bars*), and comparison with several models. The *circle* at $f=\alpha=1$ is the original non-intermittent theory of Kolmogorov (1941). The *square* at $f=\alpha=0.87$ represents the fractally homogeneous β-model of Frisch et al (1978). The two *triangles* correspond to the temporal wave-pocket model of Nakano (1988). This last model is not a cascade model. The *dashed line* is the log-normal approximation with $\mu=0.26$.

value of $f(\alpha)=1$ (showing that there is some dissipation everywhere along a line cut), and the special point $f=\alpha$, which we describe momentarily.

The multifractal description of intermittent quantities is (by and large) more general[1] than other descriptions, most of which turn out to be special cases (Figure 17). For example, Kolmogorov's (1941) space-filling dissipation corresponds to the point (1, 1) in the f-α plane. Similarly, the β-model, in which only the fraction β of the space is occupied by homogeneously distributed dissipative regions, corresponds to another point (D_β, D_β) on the plane depending on the β as well as the number of subboxes receiving the measure from the parent box. If the $f(\alpha)$ curve can be approximated by a parabola, the log-normal approximation results. (This occurs for a process whose α-distributions are random with Gaussian statistics.) As can be seen from Figure 17, log-normal approximation is not adequate except for the central portion of the curve. Low-order moments can be approximated quite well by the log-normal curves but not the high-order ones (Antonia & Sreenivasan 1977, Anselmet et al 1984). The random β-model is also inadequate because the dimension of the support in that model is less than 1.

The following are the main features of the $f(\alpha)$ distribution. For more details, the papers already cited should be consulted.

1. It should be reiterated that the $f(\alpha)$ of Figure 17 is constructed by measuring the energy dissipation rate, which (in conventional thinking) is

[1] The Kolmogorov-type reasoning is in fact more ambitious than the multifractal formalism. The former not only discusses the statistics of ε but also of the velocity field itself. For example, the 1941 theory makes a definite prediction for the velocity-derivative skewness, whereas no such predictions are possible in the multifractal picture. The derivative skewness is a dynamic quantity with special significance and cannot be predicted on the basis of dimensional or other arguments that do not invoke the Navier-Stokes equations explicitly; it is therefore no surprise that Kolmogorov's theory cannot predict it correctly.

believed to be the end-product of a cascade process. By averaging over various-sized boxes and examining the scaling properties in the range that encompasses the traditional inertial range, the expectation is to be able to extract the $f(\alpha)$ spectrum for the inertial-range analogue of ε—namely, the scale-to-scale energy flux. This can be checked as follows. Define the scaling exponents ξ_p of the moments of velocity difference ΔV_r between two points separated by a distance r as $|\Delta V_r|^p \sim r^{\xi_p}$. The scaling exponents ξ_p have been measured carefully for the inertial range by Anselmet et al (1984). On the other hand, Meneveau & Sreenivasan (1987a) have shown that the ξ_p are related to the generalized dimensions D_q as

$$\xi_p = (p/3-1)D_{p/3}+1 \tag{6.1}$$

and can be obtained as a function of p from the measured D_q data. If the measured D_q curve and the $f(\alpha)$ spectrum are inertial-range properties, then the two ways of getting the exponents ξ_p must be identical. Figure 18 compares the two sets of ξ_p. It is clear that they agree very well, justifying the earlier expectation—at least for positive moments. Note also that the log-normal distribution yields a significantly different trend.

2. Meneveau & Sreenivasan (1987a) and Sreenivasan (1990) have shown that the multifractal data are in good agreement with the measured statistical features of ε itself—for example, the Reynolds-number variation of the variance of ε (or the flatness factor of the velocity derivative). That is, for low-order moments, the same scaling that holds for the inertial range also holds approximately for the dissipation range. Indeed, the $f(\alpha)$ curves constructed for the dissipation range (Chhabra & Sreenivasan 1990b) agree for the most part with that for the inertial range.

3. Sreenivasan & Meneveau (1988) have shown that the dimension of the set of all singularities of the energy dissipation is definitely less than 1,

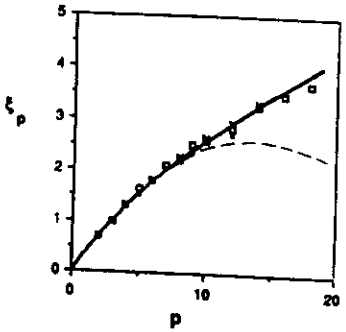

Figure 18 The scaling exponent of the velocity structure function in the inertial range. Symbols correspond to the measurements of Anselmet et al (1984), whereas the *continuous curve* is obtained from ensemble-averaged D_q results using (6.1) (from Meneveau & Sreenivasan 1987a). The *dashed curve* is for the log-normal distribution with $\mu = 0.26$.

although very close to it; the best estimate is 0.96. Most of the dissipation occurs on a subset of these singularities, whose dimension asymptotically approaches 0.87 (2.87 in three dimensions). This is the special point $f = \alpha$ mentioned earlier, corresponding to the dimension of the measure-theoretic support of ε. Since this is less than 3, all the dissipation asymptotically lives on a set of volume zero. It was argued that this set is likely to be in the form of fractal surfaces. However, the rate at which this asymptotic state is attained is very slow in Reynolds number. It may be interesting to note that the β-model assumes that the entire dissipation occurs uniformly on a set of dimension 2.87.

The set corresponding to $f = \alpha$ is inhabited by weakly singular regions (since α is not far from 1) that are quite prevalent (since f is not far from 1). It follows, asymptotically, that the entire dissipation comes from many weak peaks whose magnitudes are several orders of magnitude smaller than the rare strong ones. The latter, however, control high-order moments. The measure-theoretic supports of higher powers of ε have smaller dimensions. One can determine them from the $f(\alpha)$ curve rather easily [see (5.9)].

4. In the asymptotic limit of infinite cascade steps, one can show that the variance of box-averaged dissipation ε_r behaves as $\mu \log (L/r)$, where μ is called the intermittency exponent (see also Kolmogorov 1962). The exponent μ can be written as $\mu = -d^2\tau/dq^2|_{q=0}$. Using the measured multifractal data, Meneveau et al (1990) have shown that $\mu = 0.26 \pm 0.03$.

5. We recall from Section 3.6 that the simple estimate of 7/3 for the interface dimension did not consider fluctuations in the flux across the interface. However, fluctuations of ε cause fluctuating interface thicknesses as well as fluctuating inner cutoffs, both of which cause fluctuations in the flux. They can be accounted for in the multifractal formalism (Sreenivasan et al 1989b, Meneveau & Sreenivasan 1990a). The final result for the interface dimension is

$$D = 7/3 + 2/3(1 - D_{1/3}),$$

where $D_{1/3}$ is the generalized dimension of order 1/3. Using the measured value of $D_{1/3}$ (=0.96), one gets $D = 2.36$, in excellent agreement with the measurement (Table 1).

6. Even though the tails of the $f(\alpha)$ curve might not be entirely reliable, no reasonable extrapolation suggests the existence of the virtual part, which means that all order moments of ε are finite—putting to rest the discussion about the divergence of high-order moments of ε (Mandelbrot 1974, Schertzer & Lovejoy 1985).

7. The measured multifractal spectra have been modeled well by simple multiplicative processes (see Section 6.4).

Note that these deductions are robust against the precise partitioning of the measure [i.e. the number of offsprings arising from a parent scale (see Chhabra & Sreenivasan 1990b)].

6.2 *The Scalar Dissipation Rate*

It is important to discuss the scalar-dissipation measurements for two reasons. First, when the Schmidt number is large, there are two different scaling ranges (Section 3). Second, in the *K*-range, all three components of χ have been measured in three-dimensional space (Prasad & Sreenivasan 1990a), in a way that is closest to the ideal requirements. In Prasad et al (1988) and Ramshankar (1988), two components of χ were measured in a larger flow domain and with better resolution. In the *B*-range, Sreenivasan & Prasad (1989) measured the multifractal spectrum of the scalar dissipation by using finely resolved one-dimensional sections. Finally, there is considerable interest in χ because of its role in modeling the prediction of scalar variance and of its influence on the mean reaction rates in combustion. For example, when χ is high, extinction may occur in the flame sheet, leaving holes and pockets of unreacted, premixed mixture (Bilger 1989).

Figure 19 shows the multifractal spectrum of χ obtained from figures such as 14*b*. Since both one- and two-dimensional sections have been measured directly, checks on additive laws as well as on the existence of latent $f(\alpha)$ have been possible. Further, the results of including outer intermittency effects (or the boundary of the flow) have been investigated. These have not been included in Figure 19, since they are essentially identical to the left of the peak as well as to the right until the $f(\alpha)$ curve dips below about 1.36, this being equal to the interface dimension in planar cuts. Below this point (marked by an arrow in Figure 19), the $f(\alpha)$ curve of χ for the whole image is undefined. The interpretation appears to be that when the interface (which itself is a singularity surface) is included in the measurement of $f(\alpha)$, there are by definition no nonsingular regions: From Figure 7, it is clear that the interface occurs often enough to bias boxes of nearly all sizes. Much of the analysis done for ε has also been done for χ (Sreenivasan et al 1989a). In particular, the intermittency exponent in the *K*-range was found to be 0.36 ± 0.05, showing that χ is more intermittent than ε. Most of χ occurs on sheetlike structures of dimension close to 2.87 that occupy zero volume in the limit of infinite Reynolds number. Meneveau et al (1990) showed that the dissipation regions of χ and ε are weakly correlated, and that the scaling exponents for the structure functions of temperature obtained from the measured multifractal spectrum are consistent with direct measurements of Antonia et al 984). Mention should also be made of Ramshankar (1989), who

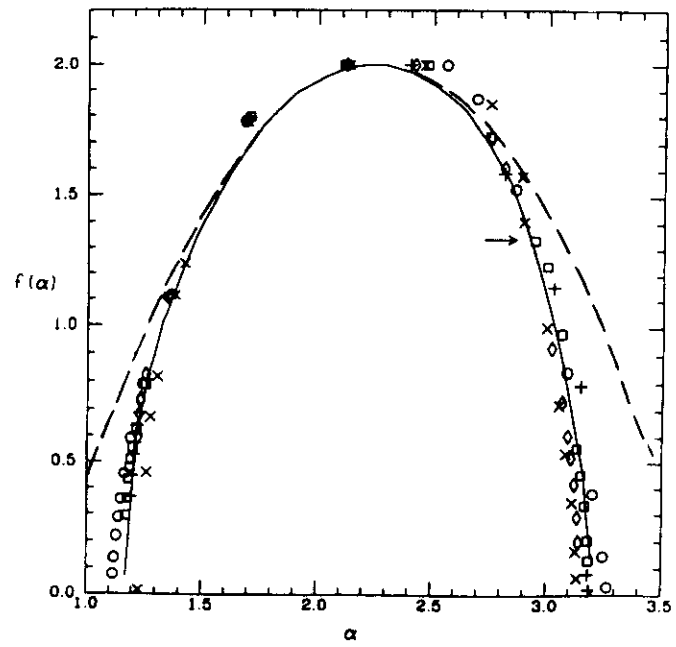

Figure 19 The $f(\alpha)$ curve for χ obtained for five different interior regions of the turbulent jet. The *continuous curve* is the average (from Prasad et al 1988). The *dashed curve* is the log-normal distribution with the scalar intermittency exponent of 0.36.

measured the Reynolds-number evolution of the multifractal spectrum for χ.

Figure 20 shows the D_q curve obtained for the *B*-range compared with that in the *K*-range [whose $f(\alpha)$ equivalent is shown in Figure 19]. The former was computed by plotting the sum of the box-averaged measures in the *B*-range and by measuring slopes. The additive law has already been invoked for the data. The generalized dimensions in the *B*-range are quite close in magnitude to that of the support. Among other things, this means that intermittency corrections in the *B*-range are negligible. As for the interface, one can expect that there are some finite Schmidt-number corrections. Sreenivasan & Prasad (1989) argued that all D_q's are identically equal to D_0 in the limit of infinite Schmidt number, and that sub-Kolmogorov-scale fluctuations are indeed space filling and nonintermittent. Classical methods must be completely adequate here.

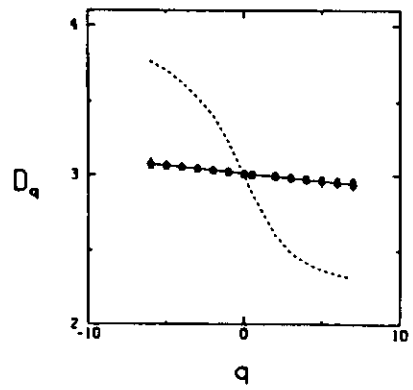

Figure 20 The generalized dimensions for the scalar dissipation χ in the two scaling ranges. Symbols correspond to the *B*-range for several different realizations, and the *solid line* represents the mean. The *dashed line* shows the results of Prasad et al (1988) for the *K*-range (from Sreenivasan & Prasad 1989).

6.3 *Further Multifractal Results and Joint Multifractals*

Similar multifractal properties have been measured (although in less detail) for absolute values of vorticity fluctuations (Fan 1988, Meneveau et al 1990) and the absolute values of the Reynolds shear stress (Kailasnath 1988). (Of interest in turbulence are vorticity and the Reynolds stress *without the absolute sign*. It is unclear how one should deal effectively with intermittent processes that are both positive and negative.) Chorin (1982, 1988a, 1990) computed the dimension of the L_2 support of vorticity and found values that seem compatible with the measurements of Fan. However, this will not be discussed further. One primary difference between enstrophy and energy dissipation is that for the former the scaling appears different in the dissipative and inertial ranges. It has also been possible to demonstrate that most of the contribution to the absolute value of the Reynolds stress in the logarithmic region of the boundary layer (for example) comes from ubiquitous but small-amplitude events, rather than from some small number of powerful events.

Finally, Meneveau et al (1990) developed the theory of joint multifractals and measured joint multifractal spectra. The primary motivation for this work is the realization that a high-Reynolds-number turbulent flow subsumes several intermittent fields simultaneously, and that these fields display different degrees of correlation among them; for example, the same set supports energy and scalar dissipation rates that have some degree of correlation among them. As before, one divides the domain of interest into boxes of various sizes and computes the integrated measures, say $p_r(x)$ and $p'_r(x)$, in boxes of size r centered around the position x. One can define two local singularity strengths α and α' according to $p_r(x) \sim (r/L)^{\alpha}$ and $p'_r(x) \sim (r/L)^{\alpha'}$, and focus on joint distributions of the variables α and α'. $N(\alpha, \alpha')\, d\alpha\, d\alpha'$ will then define the number of boxes in which the variable α is in a band $d\alpha$ around α, and α' is in a band $d\alpha'$ around α'. In analogy to the usual multifractal formalism, one writes $N_r(\alpha,\alpha') \sim (r/L)^{-f(\alpha,\alpha')}$ and interprets $f(\alpha, \alpha')$ as the dimension of a set resulting from the intersection of the iso-α and iso-α' sets. The $f(\alpha, \alpha')$ surface characterizes the scaling properties of the joint distributions of the local exponents α and α'. Meneveau et al (1990) obtained the joint multifractal spectra for energy dissipation and vorticity, as well as for energy and scalar dissipation rates. They carried out an analysis of measurements and showed that many of the previously known scaling properties follow as special cases of this general formalism. In particular, the inertial-range scaling exponents for the scalar structure functions, defined analogously to those for velocity and measured by Antonia et al (1984), are consistent with joint multifractal results. A by-product of this work is the conclusion that the scalar and energy dissipations are weakly correlated, implying that the effect of mean shear on the former will always be rather large and perhaps explaining why the structure is not locally isotropic (Mestayer et al 1976, Gibson et al 1977, Sreenivasan et al 1979, Mestayer 1983).

Another area of progress (Cates & Deutsch 1987, Meneveau & Chhabra 1990) has been the recognition that $f(\alpha)$ for random isotropic processes possesses useful information on spatial correlations (since any two boxes at some cascade level — even if distant — share the same forefather at some earlier level).

6.4 *Modeling of the Measured Multifractal Distributions*

Recall that the multifractal description is only a static, or "quenched," description, and it is usually not possible to deduce dynamical models uniquely. This is the penalty we pay for restricting attention to the physical rather than the phase space. Some headway can be made by noting, as already mentioned, that the multifractal formalism has thermodynamic analogies. Specifically, then, the question is, Can one deduce something about dynamics given merely thermodynamic information?

Consider the multiplicative process in which each parent interval breaks up into a number of new subintervals; we would have at the end of n stages of the cascade a^n pieces. The general procedure is to map such a process on to an a-state n-particle spin system and find, by taking recourse to the measured multifractal properties, the appropriate transfer matrix describ-

ing the transition from the nth stage to the $(n+1)$st stage, or from an n-particle system to an $(n+1)$-particle system.[2] One then has a dynamic process yielding the observed thermodynamics. Usually, one can only get the leading approximations to the transfer matrix (Feigenbaum et al 1986). Chhabra et al (1989a) have examined the issue for dynamical systems as well as for turbulence. Not surprisingly, inversion yields nonunique solutions: There are many dynamic processes that yield the same thermodynamics. However, the more complete our knowledge of the system, the less nonunique is the inversion procedure. Meneveau & Sreenivasan (1987b) have shown that the manifest $f(\alpha)$ is in good agreement with a binomial cascade model in which a parent eddy breaks up (in one dimension) into two equal-sized eddies such that the energy flux is redistributed between its two offsprings in the ratio 7/3. This allowed Meneveau & Sreenivasan (1987b) to make several quantitative predictions (such as the Reynolds-number variation of the flatness factor of the velocity derivative); one can also compute the spectral density of ε to a good approximation (Sreenivasan 1990). An extension to multinomial models can be made to account for the latent part also (Meneveau & Sreenivasan 1990b). Another way of accounting for negative dimensions is to use random multiplier models (Chhabra & Sreenivasan 1990b). Binomial and multinomial models have been constructed for other quantities, such as the scalar dissipation rate. (In one dimension, the splitting ratio is 3/1.) Furthermore, joint binomial models, also in agreement with measurement, can be deduced from joint distributions (Meneveau et al 1990).

Because of the non-uniqueness in going from multifractals to dynamics, one cannot claim that these models represent the true dynamics of energy cascade—despite agreement with experiment. What one can say is that simple dynamical models can be constructed in such a way that their outcome is statistically the same, up to some level of approximation, as the measured results. To determine the sense in which these models represent the true dynamic picture requires more information and is an area of active research.

6.5 *Fluctuations in Scaling Exponents*

We have seen that both interface dimensions and multifractal properties show sample-to-sample fluctuations, whereas each sample (of order $10L$ in the experiments described above, but technically of order L) has a good scaling. Even in the atmosphere, where the number of cascade levels is rather large, the sample-to-sample fluctuations are quite strong.

The reason for this is believed to be that the evolution of turbulence follows a multiplicative process that is inherently probabilistic. A single sample does not exhaust the probability density function. By considering many samples, one is essentially sampling the entire probability space. This is the spirit behind supersampling.

But what type of samples is the best for supersampling? It appears that taking line cuts via Taylor's hypothesis and performing supersampling on them is not the answer. In fact, the larger the co-dimension of the intersecting space, the worse off one is. Further, the errors in box counting can accumulate with the sample size and may lead to spurious conclusions (Chhabra & Sreenivasan 1990a,b). The multiplier method alleviates such problems when the proper partitioning is known, but the situation remains unclear if the proper partitioning is unknown. On the other hand, our experience is that three- or (at the least) two-dimensional *spatial* data possess good scaling as well as convergence.

Finally, it should be said that a deterministic explanation for the fluctuations might in fact exist. At the moment, no one seems to have a clue in that direction.

7. DETAILED NATURE OF SCALE SIMILARITY IN TURBULENCE

We have seen that multifractal spectra, although rich in information content, are statistical measures that cannot give an unambiguous picture of the scale similarity prevalent in turbulent flows. It is not clear as to what precisely one should do to acquire this detailed knowledge, but we now describe one such effort (Everson et al 1990) using wavelets (e.g. Combes et al 1989). Wavelets have recently been promoted (for example, Argoul et al 1989) as possible tools for efficient decomposition of turbulent motion into eddies of various sizes. They are spatially compact objects used to detect shapes and local gradients in a given signal by performing point-by-point convolutions with the signal. There is much freedom in picking wavelets, but for simplicity one can use a generic shape such as the "Mexican hat," which is simply the Laplacian of the Gaussian function. The idea is to use wavelets of different sizes to pick out eddies of that size and examine them for scale similarity.

Before discussing the findings of Everson et al (1990) in turbulent jets, it is helpful to first describe their results on Brownian motion $U(\mathbf{x})$ in a

[2] The number of particles at the last step of the cascade is approximately equal to $\log_2(L/\eta) = 3/4 \log_2 \mathrm{Re}$ and is not very large even for geophysical flows ($\mathrm{Re} = uL/\nu$, where u is the root-mean-square velocity). For example, for atmospheric turbulence, the number of particles is of the order of 15. We are thus discussing in turbulence the statistical mechanics of systems with a small number of particles, in strong contrast to molecular dynamics.

plane, which has the self-similar property that, under magnification or contraction by a scale factor a,

$$U(\mathbf{x}) \quad \text{and} \quad (1/a)U(a\mathbf{x}) \tag{7.1}$$

are statistically indistinguishable (Mandelbrot & Van Ness 1968).

Figure 21 (see color insert) shows two-dimensional Brownian motion $U(\mathbf{x})$ generated using a scheme suggested by Mandelbrot & Van Ness (1968). Different colors in the figure represent different probabilities of finding a particle executing Brownian motion—red and black being the most probable and the least probable states, respectively. The color code on the left of the figure graduates intermediate probabilities.

How does one visually demonstrate the presence of self-similarity in this case? Everson et al (1990) performed wavelet decomposition of the data and extracted scales of different sizes. The left column of Figure 22 (see color insert) contains the wavelet transforms of Figure 21 under successively smaller scales of the wavelet, as indicated in the caption. Unlike one-dimensional records, for which a complete wavelet transform can be rendered as a single image (Argoul et al 1989), one now needs a series of images, one for each scale. To explore the idea of self-similarity, Everson et al took the results from wavelet analysis at a scale smaller than is shown in the left column of Figure 22, and enlarged parts of it to correspond to the scales displayed. The right part of Figure 22 shows these expanded patterns, each corresponding exactly to the scale used on the left counterpart. The similarity of textural patterns confirms (7.1) and shows that the wavelet transform is capable of visually displaying statistical self-similarity. Moreover, Everson et al point out that the human eye can discern such a similarity, probably performing autocorrelations in the manner suggested by Julesz (1981).

One would like to be able to apply the same analysis to turbulent flows, for example, to the velocity data in a plane. Since there is a dearth of good planar velocity data, the jet concentration data of Figure 3 have been analyzed. Direct application of the wavelet transform to the jet image makes comparison between different regions difficult because the jet spreads in the streamwise direction and there is a consequential inhomogeneity. Everson et al therefore performed the following correction for these effects before applying the wavelet transform.

Well away from the nozzle exit, similarity arguments (for example, Townsend 1956) show that the jet spreads linearly, and the characteristic axial velocity decays as the inverse distance. The Reynolds number remains constant. The characteristic concentration levels also decrease as the inverse of the streamwise distance. Everson et al applied a conformal transformation that converts a wedge to a slot and corrected for the growth

of the jet. They also normalized the image for the expected decay rate of the concentration levels. The corrected image is shown in Figure 23 (see color insert). Properties of such rescaled jets appear fractallike without the caveats of Section 3.

The top row of Figure 24 (see color insert) shows the result of wavelet analysis on this image at four scales. In contrast to the Brownian-motion images of Figure 22, the structures at different scales are in fact different. Basically, there are two types of structures in the jet, which (following Everson et al) we might call beads and strings. As the scale decreases, structures shows a transition from beadlike to stringlike behavior. The strings are highly anisotropic. The beads are of the extent of the wavelet size, and strings are sections of sheetlike structures. Application of wavelets to the three-dimensional data of Prasad & Sreenivasan (1990a) shows that the sheets possess strong three-dimensional convolutions. We have already provided some information about these sheets in Section 6.2.

Although wavelet analysis indicates the self-affine nature of the scaling transformation in the scalar field, it is useful to investigate this further by proceeding, as was done for the planar Brownian motion, through a series of magnifications. The bottom row shows expanded versions of the wavelet picture, analyzed at a scale that is 2.5 times smaller than the rightmost one on the top row, but magnified to bring parts of the picture to the same scale as those in the top row. The arrows in the bottom four pictures correspond to the one in the top-rightmost picture. The stringlike structures persist under magnification, thus emphasizing the structural change at small scales.

At least for scalars, the tendency to stretch and fold in a highly anisotropic fashion suggests that the models that assume equal splitting—no matter how well they agree with measurements—reflect the average features and not the entire physics. As in all probabilistic processes, the agreement between a model and some of the statistical measures cannot be regarded as the whole story.

8. SUMMARY AND CONCLUSIONS

We have discussed a number of examples in which fractals and multifractals have played a role in turbulence. The exploration is still in its growth phase.

Anyone who has watched a fluid in turbulent motion is aware of the wealth of its details and complexity. Presumably, the simplest equations that describe most of those features are those formulated by Navier and Stokes. One can take the attitude that solving them on the computer will tell us all we need to know. The reality is different. In all complex systems

including high-Reynolds-number turbulence, progress can be made only by abstracting the essential features of what is obviously a very rich phenomenon. The framework of Kolmogorov's (1941) theory is one such attempt. (Although these arguments have been made independently by many other illustrious people, we have essentially used Kolmogorov as the most prominent name.) In fact, the elegance and intuitive appeal of the argument have been responsible for much of the early focus on its verification. It is correct for mean values, and one can go some way with it as a working tool; its ubiquitous use in the general storehouse of turbulence work is to some extent justified.

However, it is not correct when applied to the skewness of the velocity and temperature derivatives and to high-order moments, and it blatantly ignores intermittency. The revitalization of the earlier theory in 1962 also fell short when pushed further. Its limitations are increasingly felt as the experimental and computational capability has increased. Again, the abstraction of the details of the physics is inadequate. In particular, log-normality is inadequate for high-order moments, besides being fundamentally unsound: High-order moments are governed by very rare but extremely large events that fall outside of the central-limit theorem. The multifractal formalism provides a way in which these moments can be discussed. With this formalism, it is possible to go farther than log-normality (see, for example, Figures 17–19, where the comparisons between log-normality, multifractal results, and experiment are given). But, does this represent the ultimate level of truth, even if by that we mean nothing fancier than the Navier-Stokes description? It is not clear, given the present level of experimental uncertainty about high-order moments, that multifractal scaling extends to those very rare events; the tail of the $f(\alpha)$ curve for the atmosphere is very hard to obtain with absolute accuracy, and the issue may therefore be extremely difficult to settle. At any rate, as demonstrated in Section 7, the physics of production of small scales is more complex than that assumed by simple multifractal scaling. This, however, is not an inherent limitation, and it can perhaps be accounted for satisfactorily by inventing an appropriate self-affine transformation from scale to scale; a preliminary attempt recently made by the author appears to be promising. One must also be careful to note that the multifractal arguments give no completely satisfactory solution for dynamically important quantities such as the skewness of the velocity derivative.

What have we gained? This review has shown that fractals and multifractals are useful tools when used with an awareness of their restrictions. If the three-dimensional *spatial* structure—or at least its two-dimensional section—is examined, we have been able to ascertain the existence of reasonable scaling even at moderate Reynolds numbers. (As mentioned in Section 3.2, the situation with respect to temporal data is much less certain.) We have shown the consistency of fractal scaling with several classical Reynolds-number scalings that arise out of the Kolmogorov path. We have, on certain occasions, been able to explore beyond them. We have been able to focus more on physical space and quantify in a reasonable way some of its features. Specifically, we have been able to show the following:

1. The scalar interface in the K-range appears to have approximately the same fractal structure as the vorticity interface, and the dimension is 2.36. This is much the same for cloud boundaries and, under certain conditions, flame surfaces. The property that surfaces can be characterized in this way should be useful for obtaining the scaling laws for scalar mixing (as we have outlined) and in combustion (which, as mentioned in Section 4, is being actively explored at present). Fractals can also be useful in other contexts, such as the stretching of material lines.

2. We have shown that multifractals have an overwhelming role to play in the description of the various facets of turbulence: dissipation rates, absolute values of vorticity and Reynolds stress, etc. (Although it would at some point be useful to make detailed and highly controlled measurements at very high Reynolds numbers, the basic features of the measurements discussed here appear to be reasonably robust.) We can ascertain with some confidence the asymptotic fractal properties of the distributions of these quantities. For example, to know that all the energy and scalar dissipation rates are asymptotically distributed on fractal sets of known dimension could be of some value in turbulence modeling and in providing a conceptual framework for theoretical work. It is certainly useful to know that the contribution to the mean values of intermittent quantities comes almost exclusively from weak and frequent peaks rather than from strong and rare ones. The fact that the energy and scalar dissipation are not strongly correlated is again useful in our understanding of the limitations of local isotropy of scalar fields. The multifractal formalism provides a versatile framework for pursuing the description of turbulence. It also has a formal connection with thermodynamics and statistical mechanics, thus automatically bringing us in contact with a broad field of intellectual endeavor in physics.

What have we not been able to do? We do not truly understand why fractal and multifractal scaling holds for turbulence—at least as a reasonable approximation. Indeed, there is no satisfactory explanation of how fractals arise even in model nonlinear systems. We do not understand well the source of the fluctuations in fractal dimensions and multifractal parameters and their relation to the possible dynamical scenarios. We have

not yet been able to make a good connection to fluctuations in statistical mechanics of finite-sized systems. Both of these are areas of active research and will probably be understood sooner or later.

However, the outlook for certain other aspects is not so optimistic, unless magical inspiration or breakthrough in analytical tools occurs. By focusing on the physical space, we have lost track of the dynamic evolution. We have merely been able to suggest the type of scaling that exists in a single or several independent realizations of the flow. We do not know how to infer the true dynamics from such static descriptions—although we have tried and, in some restricted sense, succeeded. But we cannot, for instance, definitively support or deny the existence of a true Richardsonian cascade. This requires different apparatuses that focus on analysis in space-time. Purely from the point of view of measurement technology, such measurements at high Reynolds numbers remain a somewhat distant hope.

Alas, such apparatuses as exist today for undertaking a study of spatially extended dynamical systems are good only for some specific low-dimensional problems. And turbulence is decidedly high-dimensional (Landau & Lifshitz 1959, Constantin et al 1985) and is spatially structured while at the same time being random. Some intelligent work can be done in modeling subspaces of turbulent flow fields, such as near the wall where the Reynolds number is inherently low (Aubry et al 1988) or in the sub-Kolmogorov-scale range where the fractal tools might in fact be unnecessary, but the tools of today are still primitive for handling the general problem of turbulence.

Will the fractal approach survive and flourish? It is trite to say that fractals by themselves cannot solve the turbulence problem whatever that may mean. To the extent that these are mere tools, the future depends on how intelligently and judiciously they are employed. But these tools have two advantages. First, they enable us to venture beyond the existing statistical tools, which are rather heavily based on central-limit-type arguments. Second, they have allowed us to enter a number of areas of nonlinear science—thought to be beyond scientific description only a few years ago—making it easier to produce connections with those other fields. And this can only be beneficial in the long run.

ACKNOWLEDGMENTS

I wish to thank my past and present collaborators in my exploration of some of the ideas discussed here. I have cited them as appropriate but should also mention them by name: A. B. Chhabra, C. Meneveau, J. Ringland, and R. R. Prasad. I also owe much to Benoit Mandelbrot for his interest, enthusiasm, and stimulating discussions, especially concerning negative dimensions. Mitchell Feigenbaum, Mark Nelkin, and Larry Sirovich are others with whom I have had helpful conversations. The manuscript was critically read by A. B. Chhabra, A. J. Chorin, D. Kyle, J. Narasimha, R. McGowen, C. Meneveau, and P. Similon, to whom I am thankful. I am also thankful to F. Gouldin and F. Brocco, who commented on a draft version of Section 4 (to the latter also for supplying most of Figure 13), and to D. Santavicca and R. Matthews for sending preprints of their combustion papers. The research reported here was largely supported by the Air Force Office of Scientific Research and the Defense Advanced Research Projects Agency (University Research Initiative). I wish to express my appreciation to the Guggenheim Foundation, whose fellowship I held during the preparation of this review.

Literature Cited

Anselmet, F., Gagne, Y., Hopfinger, E. J., Antonia, R. A. 1984. High-order velocity structure functions in turbulent shear flows. *J. Fluid Mech.* 140: 63–89

Antonia, R. A., Sreenivasan, K. R. 1977. Log-normality of temperature dissipation in a turbulent boundary layer. *Phys. Fluids* 20: 1800–4

Antonia, R. A., Phan-Thein, N., Chambers, A. J. 1980. Taylor's hypothesis and the probability density functions of temporal velocity and temperature derivatives in a turbulent flow. *J. Fluid Mech.* 100: 193–208

Antonia, R. A., Hopfinger, E. J., Gagne, Y., Anselmet, F. 1984. Temperature structure functions in turbulent shear flows. *Phys. Rev. A* 30: 2704–7

Argoul, F., Arnéodo, G., Grasseau, G., Gagne, Y., Hopfinger, E. J., Frisch, U. 1989. Wavelet analysis reveals the multifractal nature of the Richardson cascade. *Nature* 338: 51–53

Arnéodo, A., Grasseau, G., Kostelich, E. J. 1987. Fractal dimensions and $f(\alpha)$ spectrum of the Hénon attractor. *Phys. Lett. A* 124: 426–32

Aubry, N., Holmes, P., Lumley, J. L., Stone, E. 1988. The dynamics of coherent structures in the wall region of a turbulent boundary layer. *J. Fluid Mech.* 192: 115–73

Avnir, D., ed. 1989. *The Fractal Approach to Heterogeneous Chemistry*. New York: Wiley

Ball, R. C., Kingdon, R. D. 1988. The fractal dimension of clouds. Unpubl. rep., Cambridge Univ., Engl.

Barnsley, M. F. 1988. *Fractals Everywhere*. San Diego: Academic

Batchelor, G. K. 1959. Small scale variation of convected quantities like temperature in turbulent fluid. Part 1. General discussion and the case of small conductivity. *J. Fluid Mech.* 5: 113–33

Batchelor, G. K., Townsend, A. A. 1949. The nature of turbulent motion at large wave-numbers. *Proc. R. Soc. London Ser. A* 199: 238–55

Benzi, R., Paladin, G., Parisi, G., Vulpiani, A. 1984. On the multifractal nature of fully developed turbulence and chaotic systems. *J. Phys. A* 17: 3521–31

Besicovitch, A. S. 1929. On linear sets of points of fractional dimension. *Math. Ann.* 101: 161–93

Bilger, R. W. 1989. Turbulent diffusion flames. *Annu. Rev. Fluid Mech.* 21: 101–35

Billingsley, P. 1965. *Ergodic Theory and Information*. New York: Wiley

Bunde, A., Gouyet, J. F., Rosso, M. 1987. On the problem of measuring fractal dimensions of random interfaces. *J. Phys. A: Math. Gen.* 20: 6127–32

Canny, J. 1986. A computational approach to edge detection. *IEEE Trans.* 8: 679–98

Carter, P. H., Cawley, R., Licht, A. L., Yorke, J. A., Melnik, M. S. 1986 Dimension measurement from cloud radiance. In *Dimensions and Entropies in Chaotic Systems*, ed. G. Mayer-Kress, pp. 215–21. New York: Springer-Verlag

Cates, M. E., Deutsch, J. M. 1987. Spatial correlations in multifractals. *Phys. Rev. A* 35: 4907–10

Cates, M. E., Witten, T. A. 1987. Diffusion near absorbing fractals: harmonic measure exponent for polymers. *Phys. Rev. A* 35: 1809–24

Chen, T. H., Goss, L. P. 1989. Propagation and fractals of turbulent jet diffusion flames. *AIAA Pap. No. 89-2529*

Chhabra, A., Jensen, R. V. 1989. Direct determination of the $f(\alpha)$ singularity spectrum. *Phys. Rev. Lett.* 62: 1327–30
Chhabra, A., Sreenivasan, K. R. 1990a. Probabilistic multifractals and negative dimensions. In *Proc. Meet. Turbul., Newport, R.I.*, ed. L. Sirovich. New York: Springer-Verlag. In press
Chhabra, A., Sreenivasan, K. R. 1990b. Scale-invariant and base-independent multiplier distributions in turbulence. Submitted for publication
Chhabra, A. B., Jensen, R. V., Sreenivasan, K. R. 1989a. Extraction of underlying multiplicative processes from multifractals via the thermodynamic formalism. *Phys. Rev. A* 40: 4593–4611
Chhabra, A. B., Meneveau, C., Jensen, R. V., Sreenivasan, K. R. 1989b. Direct determination of the $f(\alpha)$ singularity spectrum and its application to fully developed turbulence. *Phys. Rev. A* 40: 5284–94
Chin, Y.-W., Matthews, R. D., Nichols, S. P., Kiehne, T. M. 1990a. Use of fractal geometry to model turbulent combustion in SI engines. *Combust. Sci. Technol.* In press
Chin, Y.-W., Matthews, R. D., Nichols, S. P., Kiehne, T. M. 1990b. Continued development of an SI engine model using fractal geometry. *Proc. COMODIA 90, Kyoto.* In press
Chorin, A. J. 1982. Numerical estimates of Hausdorff dimension. *J. Comput. Phys.* 46: 390–96
Chorin, A. J. 1988a. Spectrum, dimension, and polymer analogies in fluid turbulence. *Phys. Rev. Lett.* 60: 1947–49
Chorin, A. J. 1988b. Scaling laws in the vortex lattice model of turbulence. *Commun. Math. Phys.* 114: 167–76
Chorin, A. J. 1990. Vortices, turbulence, and statistical mechanics. In *Vortex Flows*, ed. K. Gustafson, J. Sethain. Philadelphia: SIAM. In press
Combes, J. M., Grossmann, A., Tchamitchian, P. 1989. *Wavelets.* Berlin: Springer-Verlag
Constantin, P. 1990. Remarks on the Navier-Stokes equations. *Proc. Meet. Turbul., Newport, R.I.*, ed. L. Sirovich. New York: Springer-Verlag. In press
Constantin, P., Foias, C., Manley, O. P., Temam, R. 1985. Determining modes and fractal dimension of turbulent flows. *J. Fluid Mech.* 150: 427–40
Corrsin, S. 1943. Investigation of flow in an axially symmetrical heated jet of air. *NACA Wartime Rep. W-94*
Corrsin, S. 1951. On the spectrum of isotropic temperature fluctuations in an isotropic turbulence. *J. Appl. Phys.* 22: 469–73
Corrsin, S., Karweit, M. 1969. Fluid line growth in grid-generated isotropic turbulence. *J. Fluid Mech.* 39: 87–96
Corrsin, S., Kistler, A. L. 1955. Free-stream boundaries of turbulent flows. *NACA Tech. Rep. 3133*
Damköhler, G. 1940. Der Einfluss der Turbulenz auf die Flammengeschwindigkeit in Gasgemishen. *Z. Elektrochem.* 46: 601–26. Transl., 1947, as *NACA TM 1112*
Dean, A., Keefe, L. 1988. Multifractal spectra in turbulent channel flow. *Proc. NASA-Ames Turbul. Res. Cent.*
Dimotakis, P. E., Lye, R. C. M., Papantoniou, D. A. 1983. Structure and dynamics of round turbulent jets. *Phys. Fluids* 26: 3185–92
Eggelston, H. G. 1949. The fractional dimension of a set defined by decimal properties. *Q. J. Math.* 20: 31–36
Everson, R., Sirovich, L., Sreenivasan, K. R. 1990. Wavelet analysis of the turbulent jet. *Phys. Lett. A* 145: 314–22
Falconer, K. J. 1984. *The Geometry of Fractal Sets.* Cambridge: Univ. Press
Fan, M. S. 1988. The multifractal nature of the turbulent streamwise vorticity measured in wind tunnel flows and atmospheric flow. *Fluid Mech. Rep. 12*, Yale Univ., New Haven, Conn.
Feder, J. 1988. *Fractals.* New York: Plenum
Feigenbaum, M. J. 1978. Quantitative universality for a class of nonlinear transformations. *J. Stat. Phys.* 19: 25–52
Feigenbaum, M. J. 1987a. Some characterizations of strange sets. *J. Stat. Phys.* 46: 919–24
Feigenbaum, M. J. 1987b. Scaling spectra and return times of dynamical systems. *J. Stat. Phys.* 46: 925–32
Feigenbaum, M. J., Jensen, M. H., Procaccia, I. 1986. Time ordering and the thermodynamics of strange sets: theory and experimental tests. *Phys. Rev. Lett.* 57: 1503–6
Frisch, U., Orszag, S. A. 1990. Turbulence: challenges for theory and experiment. *Phys. Today* 43: 24–32
Frisch, U., Parisi, G. 1985. On the singularity structure of fully developed turbulence. In *Turbulence and Predictability in Geophysical Fluid Dynamics and Climate Dynamics*, ed. M. Ghil, R. Benzi, G. Parisi, pp. 84–88. Amsterdam: North-Holland
Frisch, U., Sulem, P.-L., Nelkin, M. 1978. A simple dynamical model of intermittent fully developed turbulence. *J. Fluid Mech.* 87: 719–36
Gibson, C. H., Friehe, C., McConnell, S. O. 1977. Structure of sheared turbulent fields. *Phys. Fluids* 20: 5156–57
Goix, P. J., Shepherd, I. G., Trinite, M. 1989.

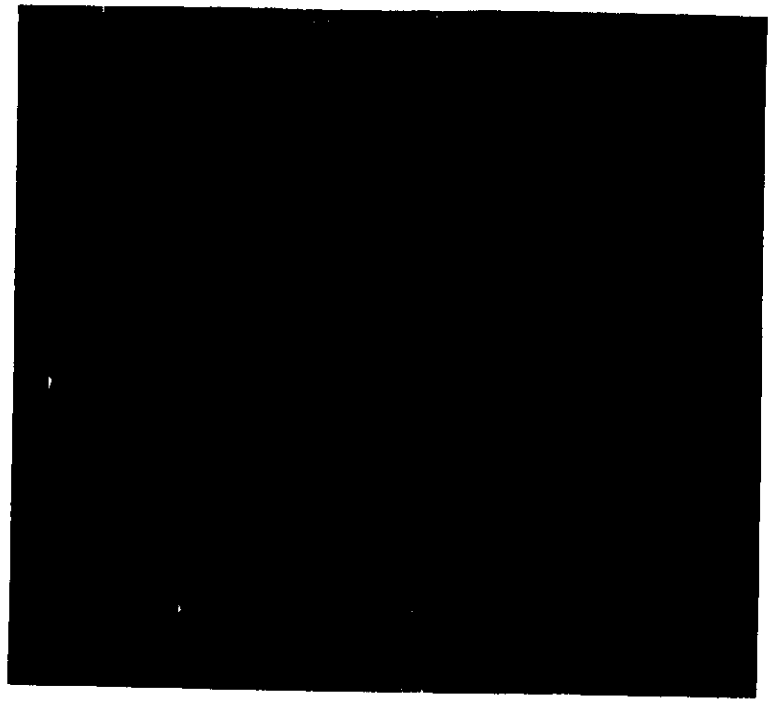

Figure 14a From the LIF map of the concentration field, one can calculate the "dissipation" rate of the variance of concentration fluctuation. This is shown for one realization of a jet at a Reynolds number of 4000. The gradients of the concentration required for computing χ were approximated by finite differences of the concentration field. Only two components of χ are included here. The spatial resolution of measurements is estimated to be between $\langle\eta\rangle$ and $2\langle\eta\rangle$. Different colors represent, in some nonlinear scaling, different magnitudes of the dissipation rate; magnitudes increase from deep blue through red. The figure shows that different magnitudes of dissipation inhabit different but intertwined sets. The purpose of the multifractal analysis is to disentangle information about the dimensions of these sets and the strengths of the measures living on them.

Figure 21 A Brownian surface in a plane generated according to the scheme suggested by Mandelbrot & Van Ness (1968). A linear cut of this surface gives the Brownian motion on a line. The spatial spectrum falls off according to the second power of the wavenumber. Different colors represent different probabilities, or heights of the Brownian surface (from Everson et al 1990).

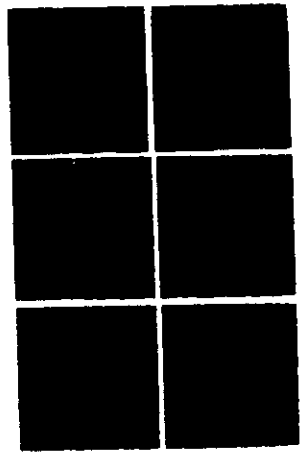

Figure 22 Wavelet transform, at scale a, of the Brownian motion displayed in Figure 21. The left column, going from top to bottom, corresponds to $a = 0.1$, $a = 0.05$, and $a = 0.01$. Right column, from top to bottom: $a = 0.05$, magnified 2 times; $a = 0.02$, magnified 2.5 times; $a = 0.005$, magnified 2 times. The linear dimension of each picture in the left column corresponds to $a = 1$ (from Everson et al 1990).

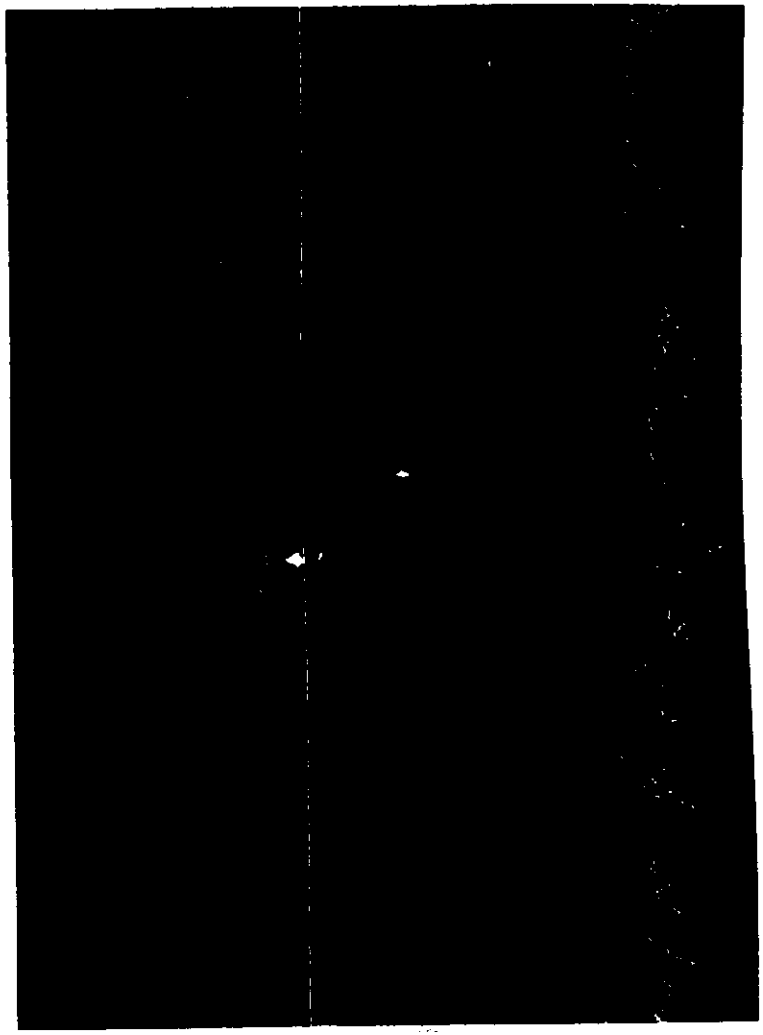

Figure 23 The result of applying a conformal mapping to the jet shown in Figure 3. The map, due to Everson et al (1990), corrects for the growth of the jet by coverting a wedge into a slot. The downstream decay of the mean concentration has been normalized using similarity considerations. The signal to the right corresponds to the vertical line cut shown in the jet.

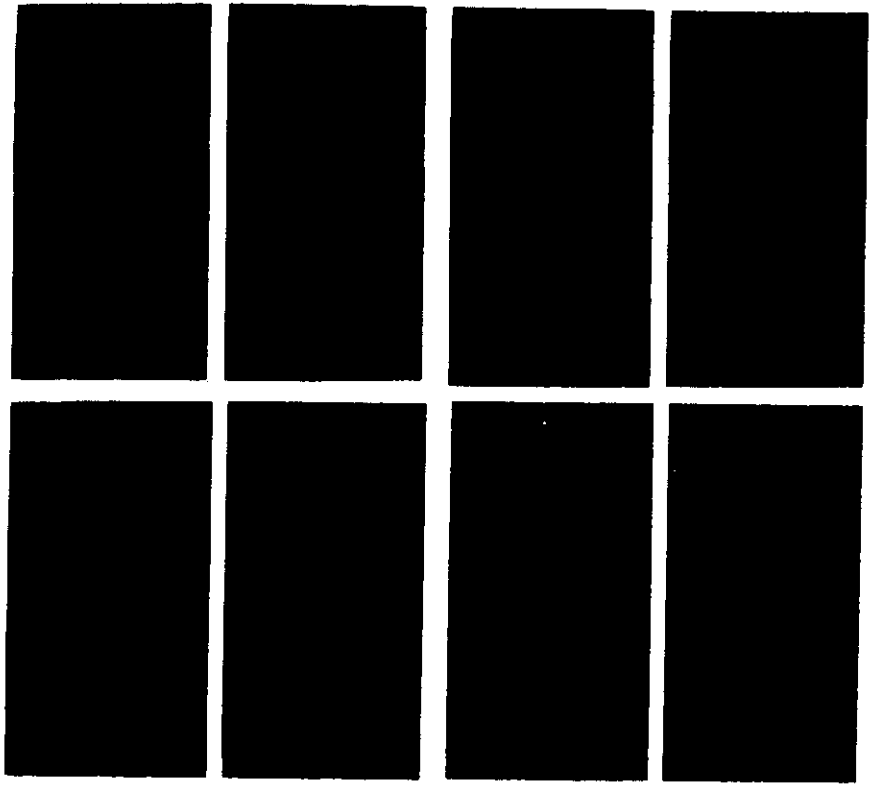

Figure 24 Wavelet transform of the (mirror image of the) conformally mapped jet shown in Figure 23. Scale sizes across top row are $a = 0.05$, 0.02, 0.01, and 0.005. The longer dimension of the picture corresponds to $a = 1$. The bottom row, going from left to right: $a = 0.002$, magnified 25 times; $a = 0.002$, magnified 10 times; $a = 0.002$, magnified 5 times; $a = 0.002$, magnified 2.5 times. The location of the magnified region is indicated by arrows, which point to the same features in each picture. Focusing on other regions gives essentially the same qualitative picture. It is clear that scale similarity for the Brownian motion is different from that for the scalar structure in this jet (and, it appears, in other sheared flows) (from Everson et al 1990).

A fractal study of a premixed V-shaped H_2/air flame. *Combust. Sci. Technol.* 63: 275–86

Gouldin, F. C. 1987. An application of fractals to modeling premixed turbulent flames. *Combust. Flame* 68: 249–66

Gouldin, F. C. 1988. Interpretation of jet mixing using fractals. *AIAA J.* 26: 1405–7

Gouldin, F. C., Hilton, S. H., Lamb, T. 1988. Experimental evaluation of the fractal geometry of flamelets. *Int. Symp. Combust., 22nd*, pp. 541–50. Pittsburgh: Combust. Inst.

Gouldin, F. C., Bray, K. N. C., Chen, J.-Y. 1989. Chemical closure model for fractal flamelets. *Combust. Flame* 77: 241–59

Halsey, T. C., Jensen, M. H., Kadanoff, L. P., Procaccia, I., Shraiman, B. I. 1986 Fractal measures and their singularities the characterization of strange sets. *Phys. Rev. A* 33: 1141–51

Hausdorff, F. 1919. Dimension und ausseres Mass. *Math. Ann.* 29: 157–79

Hawkes, J. 1974. Hausdorff measure, entropy and the independence of small sets. *Proc. London Math. Soc.* 28: 700–24

Hentschel, H. G. E., Procaccia, I. 1983. The infinite number of generalized dimensions of fractals and strange attractors. *Physica D* 8: 435–44

Hentschel, H. G. E., Procaccia, I. 1984. Relative diffusion in turbulent media: the fractal dimension of clouds. *Phys. Rev. A* 29: 1461–70

Jensen, M. H., Kadanoff, L. P., Libchaber, A., Procaccia, I., Stavans, J. 1985. Global universality at the onset of chaos: results of a forced Rayleigh-Benard experiment. *Phys. Rev. Lett.* 55: 2798–2801

Johnson, A. 1989. Mixing and the fractal description of a turbulent boundary layer in supersonic flow. *Fluid Mech. Rep. 5*, Yale Univ., New Haven, Conn.

Julesz, B. 1981. Textrons, the elements of texture perception and their interaction. *Nature* 290: 91–97

Kailasnath, P. 1988. Some aspects of the structure of the Reynolds stress in a turbulent boundary layer and the analogy with the energy cascade ideas of turbulence. *Fluid Mech. Rep. 18*, Yale Univ., New Haven, Conn.

Kerr, R. M. 1985. Higher-order derivative correlations and the alignment of small-scale structures in isotropic numerical turbulence. *J. Fluid Mech.* 153: 31–58

Kolmogorov, A. N. 1941. Local structure of turbulence in an incompressible fluid at very high Reynolds numbers. *Dokl. Akad. Nauk SSSR* 30: 299–303

Kolmogorov, A. N. 1962. A refinement of previous hypotheses concerning the local structure of turbulence in a viscous incompressible fluid at high Reynolds number. *J. Fluid Mech.* 13: 82–85

Kraichnan, R. H. 1974. On Kolmogorov's inertial-range theories. *J. Fluid Mech.* 62: 305–30

Kuo, A. Y.-S., Corrsin, S. 1972. Experiment on the geometry of the fine-structure regions in fully turbulent fluid. *J. Fluid Mech.* 56: 447–79

Landau, L. D., Lifshitz, E. M. 1959 *Fluid Mechanics*. Oxford: Pergamon

Levich, E. 1987. Certain problems in the theory of developed hydrodynamic turbulence. *Phys. Rep.* 151: 129–238

Libby, P. A. 1974. Analytical and numerical methods for the investigation of flow fields with chemical reactions, especially related to combustion. *AGARD Conf. Proc.* 164[11]: 5–8

Libby, P. A., Williams, F. A. 1976. Turbulent flows involving chemical reactions. *Annu. Rev. Fluid Mech.* 8: 351–76

Liepmann, D., Gharib, M. 1985. Fractal dimension transition in a round jet. *Bull. Am. Phys. Soc.* 32: 2067 (Abstr.)

Lovejoy, S. 1982. Area-perimeter relation for rain and cloud areas. *Science* 216: 185–87

Lovejoy, S., Mandelbrot, B. B. 1985. Fractal properties of rain, and a fractal model. *Tellus* 37A: 209–32

Lovejoy, S., Schertzer, D. 1985. Generalized scale-invariance in the atmosphere and fractal models of rain. *Water Resour. Res.* 21: 1233–50

Lumley, J. L. 1965. Interpretation of time spectra measured in high-intensity shear flows. *Phys. Fluids* 8: 1056–62

Mandelbrot, B. B. 1972. Possible refinement of the lognormal hypothesis concerning the distribution of energy dissipation in intermittent turbulence. In *Statistical Models and Turbulence*, ed. M. Rosenblatt, C. W. Van Atta, pp. 333–51. New York: Springer-Verlag

Mandelbrot, B. B. 1974. Intermittent turbulence in self-similar cascades: divergence of high moments and dimension of the carrier. *J. Fluid Mech.* 62: 331–58

Mandelbrot, B. B. 1982. *The Fractal Geometry of Nature*. San Francisco: Freeman

Mandelbrot, B. B. 1984. Fractals in physics: squid clusters, diffusions, fractal measures, and the unicity of fractal dimensionality. *J. Stat. Phys.* 34: 895–930

Mandelbrot, B. B. 1985. Self-affine fractals and fractal dimension. *Phys. Scr.* 32: 257–60

Mandelbrot, B. B. 1986. Self-affine fractal sets. In *Fractals in Physics*, ed. L. Pietronero, E. Tosatti, pp. 3–28. Amsterdam: North-Holland

Mandelbrot, B. B. 1989a. Fractal geometry:

what is it, and what does it do? *Proc. R. Soc. London Ser. A* 423: 3–16
Mandelbrot, B. B. 1989b. Multifractal measures, especially for the geophysicist. *Pure Appl. Geophys.* 131: 5–42
Mandelbrot, B. B., Scholz, C. H., eds. 1989. *Fractals in Geophysics. Pure Appl. Geophys.*, Vol. 131. Boston: Birkhauser
Mandelbrot, B. B., Van Ness, J. W. 1968. Fractional Brownian motion, fractional noises and applications. *SIAM Rev.* 10: 422–37
Mantzaras, J., Felton, P. G., Bracco, F. V. 1989a. Fractals and turbulent premixed engine flames. *Combust. Flame* 77: 295–310
Mantzaras, J., Felton, P. G., Bracco, F. V. 1989b. Is laminar flame front a passive scalar surface of the turbulent field? *ASCE/ASME Mech. Conf., 3rd, San Diego*
Marstrand, J. M. 1954. Some fundamental geometrical properties of plane sets of fractional dimension. *Proc. London Math. Soc.* 4: 257–302
Mattila, P. 1975. Hausdorff dimension, orthogonal projections and intersections with planes. *Ann. Acad. Sci. Fenn. Ser. A. Math.* 1: 227–44
Maxwell, J. C. 1879. Thomson and Tait's natural philosophy. *Nature* 20: 213–16
McCauley, J. L. 1989. Statistical mechanics of multifractals. Preprint (Univ. Houston, Tex.)
Meneveau, C., Chhabra, A. 1990. Two-point statistics of multifractal measures. *Physica A* 164: 564–74
Meneveau, C., Sreenivasan, K. R. 1987a. The multifractal spectrum of the dissipation field in turbulent flows. *Nucl. Phys. B (Proc. Suppl.)* 2: 49–76
Meneveau, C., Sreenivasan, K. R. 1987b. Simple multifractal cascade model for fully developed turbulence. *Phys. Rev. Lett.* 59: 1424–27
Meneveau, C., Sreenivasan, K. R. 1989. Measurement of $f(\alpha)$ from scaling of histograms and applications to dynamical systems and fully developed turbulence. *Phys. Lett. A* 137: 103–12
Meneveau, C., Sreenivasan, K. R. 1990a. Interface dimension in intermittent turbulence. *Phys. Rev. A* 41: 2246–48
Meneveau, C., Sreenivasan, K. R. 1990b. The multifractal nature of the turbulent energy dissipation. *J. Fluid Mech.* In press
Meneveau, C., Sreenivasan, K. R., Kailasnath, P., Fan, S. 1990. Joint multifractal measures: theory and applications to turbulence. *Phys. Rev. A* 41: 894–914
Mestayer, P. G. 1983. Local isotropy and anisotropy in a high-Reynolds-number turbulent boundary layer. *J. Fluid Mech.* 125: 475–503
Mestayer, P. G., Gibson, C. H., Coantic, M. F., Patel, A. S. 1976. Local anisotropy in heated and cooled turbulent boundary layers. *Phys. Fluids* 19: 1279–87
Monin, A. S., Yaglom, A. M. 1971. *Statistical Fluid Mechanics*, Vol. 2. Cambridge, Mass: MIT Press
Murayama, M., Takeno, T. 1988. Fractal-like character of flamelets in turbulent premixed combustion. *Int. Symp. Combust., 22nd*, pp. 551–59. Pittsburgh: Combust. Inst.
Nakano, T. 1988. Determination of a dynamical scaling function in a cascade model of turbulence. *Prog. Theor. Phys.* 79: 569–80
Nelkin, M. 1989. What do we know about self-similarity in fluid turbulence? *J. Stat. Phys.* 54: 1–15
North, G. L., Santavicca, D. A. 1990. The fractal nature of premixed turbulent flames. *Combust. Sci. Technol.* In press
Novikov, E. A. 1969. Scale-similarity for random fields. *Sov. Phys. Dokl.* 14: 104–7
Novikov, E. A. 1970. Intermittency and scale similarity in the structure of a turbulent flow. *Prikl. Mat. Mekh.* 35: 266–77
Novikov, E. A., Stewart, R. W. 1964. Intermittency of turbulence and the spectrum of fluctuations of energy dissipation. *Izv. Akad. Nauk SSSR, Ser. Geofiz.* 3: 408–13
Obukhov, A. M. 1949. Structure of the temperature field in a turbulent flow. *Izv. Akad. Nauk SSSR, Ser. Fiz.* 6: 1–2, 59–63
Obukhov, A. M. 1962. Some specific features of atmospheric turbulence. *J. Fluid Mech.* 13: 77–81
Olinger, D. J., Sreenivasan, K. R. 1988. Nonlinear dynamics of the wake of an oscillating cylinder. *Phys. Rev. Lett.* 60: 797–800
Orszag, S. A. 1970. Indeterminacy of the moment problem for intermittent turbulence. *Phys. Fluids* 13: 2211–12
Peters, N. 1986. Laminar flamelet concepts in turbulent combustion. *Int. Symp. Combust., 21st*, pp. 1232–50. Pittsburgh: Combust. Inst.
Pietronero, L., ed. 1989. *Fractals*. New York: Plenum
Pope, S. B. 1987. Turbulent premixed flames. *Annu. Rev. Fluid Mech.* 19: 237–70
Prasad, R. R., Sreenivasan, K. R. 1988. Fractal facets of axisymmetric jets. In *Gallery of Fluid Motion*, compil. H. L. Reed. *Phys. Fluids* 31: 2383–94
Prasad, R. R., Sreenivasan, K. R. 1989. Scalar boundaries in digital images of turbulent flows. *Exp. Fluids* 7: 259–64
Prasad, R. R., Sreenivasan, K. R. 1990a. Quantitative three-dimensional imaging and the structure of passive scalar fields in fully turbulent flows. *J. Fluid Mech.* 216: 1–34

Prasad, R. R., Sreenivasan, K. R. 1990b. The measurement and interpretation of fractal dimensions of surfaces in turbulent flows. *Phys. Fluids A* 2: 792–807
Prasad, R. R., Meneveau, C., Sreenivasan, K. R. 1988. The multifractal nature of the dissipation field of passive scalars in fully turbulent flows. *Phys. Rev. Lett.* 61: 74–77
Ramshankar, R. 1988. *The dynamics of countercurrent mixing layers*. PhD thesis. Yale Univ., New Haven, Conn.
Ramshankar, R. 1989. Mixing in temporally developing shear layers: the multifractal approach. *Proc. Forum Chaotic Dyn. ASME Fluids Eng. Conf., La Jolla, Calif.*
Redondo, J., Linden, P. F. 1988. The fractal dimension of stratified turbulence. Preprint (Dep. Appl. Math. Theor. Phys., Univ. Cambridge)
Richardson, L. F. 1922. *Weather Prediction by Numerical Process*. Cambridge: Univ. Press
Rys, F. S., Waldvogel, A. 1986. Fractal shape of hail clouds. *Phys. Rev. Lett.* 56: 784–87
Santavicca, D. A., Liou, D., North, G. L. 1990. A fractal model of turbulent flame kernel growth. *SAE Tech. Pap. No. 900024*. Eng. Soc. Adv. Mobility Land Sea Air and Space, pp. 1–9
Saylor, J. 1989. Segmentation of flow visualization images. *Fluid Mech. Rep. 19*, Yale Univ., New Haven, Conn.
Schertzer, D., Lovejoy, S. 1985. The dimension and intermittency of atmospheric dynamics. In *Turbulent Shear Flows 4*, ed. B. Launder, pp. 7–33. New York: Springer-Verlag
Sreenivasan, K. R. 1990. The utility of dynamical systems approach, comment 3. In *Whither Turbulence? Turbulence at Cross-Roads*, ed. J. L. Lumley, pp. 269–91. New York: Springer-Verlag
Sreenivasan, K. R., Aronstein, D. 1985. The fractal geometry of turbulence. *Bull. Am. Phys. Soc.* 30: 1702 (Abstr.)
Sreenivasan, K. R., Meneveau, C. 1986. The fractal facets of turbulence. *J. Fluid Mech.* 173: 357–86
Sreenivasan, K. R., Meneveau, C. 1988. Singularities of the equations of fluid motion. *Phys. Rev. A* 38: 6287–95
Sreenivasan, K. R., Prasad, R. R. 1989. New results on the fractal and multifractal structure of the large Schmidt number passive scalars in fully turbulent flows. *Physica D* 38: 322–29
Sreenivasan, K. R., Antonia, R. A., Britz, D. 1979. Local isotropy and large structure in a heated turbulent jet. *J. Fluid Mech.* 94: 745–75
Sreenivasan, K. R., Prabhu, A., Narasimha, R. 1983. Zero-crossings in turbulent signals. *J. Fluid Mech.* 137: 251–72
Sreenivasan, K. R., Prasad, R. R., Meneveau, C., Ramshankar, R. 1989a. The fractal geometry of interfaces and the multifractal distribution of dissipation in fully turbulent flows. See Mandelbrot & Scholz, pp. 43–60
Sreenivasan, K. R., Ramshankar, R., Meneveau, C. 1989b. Mixing, entrainment, and fractal dimension of surfaces in turbulent flow. *Proc. R. Soc. London Ser. A* 421: 79–108
Stanley, H. E., Ostrowsky, N., eds. 1985. *On Growth and Form: Fractal and Non-Fractal Patterns in Physics*. Boston Dordrecht: Nijhoff-Kluwer
Strahle, W. C., Jagoda, J. I. 1988. Fractal geometry application in turbulent combustion data analysis. *Int. Symp. Combust., 22nd*, pp. 561–88. Pittsburgh: Combust. Inst.
Tabeling, P. 1985. Sudden increase of the fractal dimension in a hydrodynamic system. *Phys. Rev. A* 31: 3460–62
Tong, P., Goldburg, W. I. 1988. Experimental study of relative velocity fluctuations in turbulence. *Phys. Lett. A* 127: 147–50
Townsend, A. A. 1956. *The Structure of Turbulent Shear Flows*. Cambridge: Univ. Press
Turcotte, D. L. 1988. Fractals in fluid mechanics. *Annu. Rev. Fluid Mech.* 20: 5–16
Van de Water, W., Schram, P. 1988. Generalized dimensions from near-neighbor information. *Phys. Rev. A* 37: 3118–25
Van Damme, H., Obrecht, F., Levitz, P., Gatineau, L., Laroche, C. 1986. Fractal viscous fingering in clay slurries. *Nature* 320: 731–33
Vassilicos, J. C. 1989. On the geometry of lines in two-dimensional turbulence. In *Advances in Turbulence 2*, ed. H.-H. Fernholtz, H. E. Fiedler, pp. 404–11. Berlin: Springer-Verlag
Vicsek, T. 1989. *Fractal Growth Phenomena*. Singapore: World Sci.
Voss, R. F. 1989. Random fractals: self-affinity in noise, music, mountains, and clouds. *Physica D* 38: 362–71
Ware, B. R., Cyr, D., Gorti, S., Lanni, F. 1983. Electrophoretic and frictional properties of particles in complex media measured by laser light scattering and fluorescence photobleaching recovery. In *Measurement of Suspended Particles by Quasi-Elastic Light Scattering*, ed. B. F. Dahneke, pp. 255–89. New York: Wiley

NOTE ADDED IN PROOF As we go to press, three further comments might usefully be added. First, Miller & Dimotakis (1991) have confirmed the conclusion of Section 3.2 that *temporal* records of concentration in a jet do not have a fractal character, at least for thresholds near the mean. Their results for threshold levels far from the mean are less clear (see their Figures 11, 12). The work highlights the difficulty in treating one-dimensional temporal records, which are inherently self-affine, in terms of self-similar fractals. Miller & Dimotakis have not examined spatial records, to which most of this review refers, but they do find that small extents of streak images (i.e. images obtained by treating temporal signals from a line array of diode elements as spatial images) show no evidence of fractal behavior. This result deserves attention, even though the use of Taylor's hypothesis in two dimensions remains an unexplored domain.

Second, Vassilicos & Hunt (1990) have shown that spiral shapes satisfying certain geometric constraints possess a capacity dimension equal to the measured value of ~ 2.35 for the scalar interface. On the basis of this and other evidence, they speculate that turbulent motion may indeed consist of many spiraling motions. While we do observe some spiral structures (with a few turns of order 2) in the small-scale scalar field, they are not ubiquitous, and reality appears to be much more complex.

Finally, Barcy et al (1990) and U. Frisch (private communication, 1989) have argued that generalized dimension D_q for $q < 1$ cannot exist for the dissipation field. This may indeed be the case, but measurements discussed in Section 5 are for box-averaged dissipation whose scaling for negative q extends only to some multiple of the Kolmogorov scale—that is, coarse-grained dissipation and the dissipation per se may have different characteristics as far as negative q's are concerned. As explained in the text, the hope (which a posteriori appears to be justified) is that one may be able to extract inertial-range quantities by box averaging dissipation quantities. While there is no guarantee that this view is exactly right, evidence presented in the text shows that this might be sufficiently correct for positive moments.

Barcy, E., Arneodo, A., Frisch, U., Gagne, Y., Hopfinger, E. 1990. Wavelet analysis of fully developed turbulence data and measurement of scaling exponents. In *Turbulence and Coherent Structures*, ed. M. Lesieur, G. Metais. Dordrecht: Kluwer. In press

Miller, P. L., Dimotakis, P. E. 1991. Stochastic geometric properties of scalar interface in turbulent jets. *Phys. Fluids A*. In press

Vassilicos, J. C., Hunt, J. C. R. 1990. Kinematics of small-scale motion in homogeneous isotropic turbulence. *Proc. Eur. Turbul. Conf., 3rd*, ed. A. Johansson, P. H. Alfredsson. Berlin: Springer-Verlag. In press